

UNIVERSITY OF WROCLAW

MASTER THESIS

Impact of Correlated Nucleon Pairs on Neutrino-Nucleus Interactions

Author:
Kajetan NIEWCZAS

Supervisor:
prof. dr hab. Jan SOBCZYK

*A thesis submitted in fulfilment of the requirements
for the degree of Master of Science*

in the

Faculty of Physics and Astronomy
University of Wrocław

September 2016



Uniwersytet
Wrocławski

Abstract

Faculty of Physics and Astronomy
University of Wrocław

Master Thesis

Impact of Correlated Nucleon Pairs on Neutrino-Nucleus Interactions

by Kajetan NIEWCZAS

This thesis is an introduction to the analysis of the role of nucleon correlations in lepton-nucleus interactions. The theoretical foundation for this discussion is presented through the example of an electron scattering off a free nucleon target. Then, the analysis is extended to the problem of complex hadronic targets. The electron-nucleus cross section is considered in various approximative regimes: namely, the *impulse approximation* (IA), *plane wave impulse approximation* (PWIA) and the *relativistic plane wave impulse approximation* (RPWIA). The discussion about the theoretical foundation is finished with a discussion about two-body current interactions and the issues therein. The remainder of this thesis is devoted to the correlated nucleon pairs within nuclear targets. The theoretical approaches are presented. Then, the role of short-range nucleon-nucleon correlations in the ArgoNeuT experimental data [Phys. Rev. D90 (2014) 012008] is investigated with the NuWro Monte Carlo (MC) event generator. An attempt is made to estimate how likely it is to obtain observed or back-to-back nucleon pairs in the lab frame, as well as reconstructed ones. For laboratory frame back-to-back events a clear data/MC discrepancy is seen. For the reconstructed nucleon pairs, a good agreement is reported. A kinematical argument for why this accordance is expected is provided.

Streszczenie

Wydział Fizyki i Astronomii
Uniwersytet Wrocławski

Praca Magisterska

Wpływ skorelowanych par nukleonów na proces rozpraszania neutrin na jądrach atomowych

Kajetan NIEWCZAS

Praca jest wprowadzeniem do analizy wpływu skorelowanych par nukleonów na proces rozpraszania leptonów na jądrach atomowych. Wstęp do opisu teoretycznego opiera się na przykładzie rozpraszania elektronów na swobodnych nukleonach. Następnie analiza zostaje rozszerzona do problemu rozpraszania elektronów na jądrach atomowych. Przekrój czynny na reakcję elektron-jądro rozpatrywany jest w trzech przypadkach: przybliżenia impulsowego, przybliżenia impulsowego fali płaskiej oraz relatywistycznego przybliżenia impulsowego fali płaskiej. Ta część pracy jest zakończona dyskusją na temat oddziaływań przez prądy dwuciałowe. Druga część pracy dotyczy badań nad skorelowanymi parami nukleonów w tarczach jądrowych. Omówione są tu wybrane prace teoretyczne. Następnie przeanalizowane są odkrycia eksperymentu ArgoNeuT [Phys. Rev. D90 (2014) 012008] z użyciem danych symulacji Monte Carlo (MC) generatora NuWro. Na gruncie symulacji MC, podjęto próbę oszacowania prawdopodobieństwa otrzymania określonych rozkładów kątów pomiędzy wybitymi protonami w układzie laboratoryjnym oraz pomiędzy protonami w zrekonstruowanej konfiguracji początkowej. Dla kątów w układzie laboratoryjnym znaleziono rozbieżność pomiędzy danymi eksperymentalnymi oraz symulacją NuWro. Dla zrekonstruowanych konfiguracji dane eksperymentalne pokrywały się z wynikami symulacji. Dyskusję kończy kinematyczny argument wyjaśniający taki wynik.

Acknowledgements

I would like to thank my supervisor, prof. dr hab. Jan Sobczyk, for his friendly guidance and wise advices.

I am also very much thankful to my fiancée, Aleksandra, for all of her support and kindness.

I acknowledge with thanks the comments that I recieved from Michał Marczenko that helped in writing this thesis.

I would also like to thank my colleagues: Mateusz Bancewicz, Mark Alexander Randolph Kaltenborn, Łukasz Juchnowski, Pok Man Lo, Michał Szymański and Mateusz Cierniak for all of the fruitful discussions and friendly atmosphere during those 5 years.

Last but not at least, I express my sincere gratitude to my parents and Zbigniew for all their support.

Abbreviations

CCQE	C arged C urrent Q uasi E lastic
DIS	D eep I nelastic S cattering
FNAL	F ermi N ational A ccelerator L aboratory
FG	F ermi G as
FSI	F inal S tate I nteractions
IA	I mpulse A pproximation
INC	I ntra N uclear C ascade
IP	I ndependent P article
ISC	I nitial S tate C orrelations
LArTPC	L iquid A rgon T ime P rojection C hamber
LFG	L ocal F ermi G as
MC	M onte C arlo
MEC	M eson E xchange C urrent
PWIA	P lane W ave I mpulse A pproximation
RES	R ESonant
SF	S pectral F unction
SM	S tandard M odel
SRC	S hort- R ange C orrelation
TPC	T ime P rojection C hamber
QED	Q uantum E lectro D ynamics
QFT	Q uantum F ield T heory

Contents

Abstract	i
Acknowledgements	iii
Abbreviations	iv
Contents	v
Introduction	0
1 Electron-nucleon scattering	5
1.1 Introduction	6
1.2 Differential cross section	7
1.3 Electromagnetic form factors	10
1.4 Tensor contraction	11
1.5 Interpretation	13
2 Electron-nucleus scattering	17
2.1 Introduction	18
2.2 Impulse Approximation	19
2.2.1 One-body current	20
2.2.2 Hadronic tensor	20
2.3 Plane wave IA	22
2.3.1 Factorization	23
2.3.2 Spectral function	24
2.3.3 Factorized cross section	25
2.3.4 Specific nucleon solution	27
2.4 Relativistic PWIA	29
2.4.1 One-body current	30
2.4.2 Hadronic tensor	30
2.4.3 Spectral functions	31
2.4.4 Specific nucleon solution	32
2.5 Two-body interaction	34
3 Correlated nucleon pairs and the two-nucleon knockout	37
3.1 Short-range correlated nucleon pairs	39
3.2 Theoretical approaches	40

3.3	ArgoNeuT experiment	41
3.4	NuWro simulations	42
3.4.1	NuWro configurations	43
3.4.2	Normalization	45
3.4.3	Finite detector size	46
3.4.4	Two proton events	46
3.5	Hammer events in the laboratory frame	48
3.6	Reconstructed back-to-back nucleons before interaction	51
3.7	Discussion	54
3.7.1	Missing transverse momentum	54
3.7.2	Kinematics reconstruction procedure	56
	Conclusions	62
	A Notation and conventions	65
A.1	Covariant notation	65
A.2	Dirac equation	66
A.3	Normalization	67
	B Cross section	71
B.1	Simple cross section definition	71
B.2	Quantization in the finite volume	72
B.3	Feynman rules in QED	74
	C Electron-nucleon scattering	77
C.1	Dirac delta integration	77
C.2	Leptonic tensor calculation	79
C.3	Hadronic tensor calculation	79
C.4	Tensor contraction	82
	Bibliography	85

Introduction

The existence of an elusive particle referred to as the neutrino was proposed by W. Pauli on December 4th, 1930 [1]. Although considered undetectable, its experimental confirmation came in 1956 with an experiment led by C. L. Cowan and F. Reines [2]. Neutrino physics has been one of the most rapidly growing branches of particle physics ever since. Nowadays, neutrinos are considered as one of the building blocks of the Standard Model (SM) as the only electrically neutral fermions. In the lowest order, they do not participate in the electromagnetic interaction and interact only weakly (by the exchange of the virtual W^\pm and Z^0 bosons). Their masses, not included in the SM, are significantly smaller than the masses of charged leptons and quarks. These traits make neutrinos extremely elusive particles; they cause yet many surprising phenomena. For more details on both the history and properties of neutrinos see, e.g., [3] and the references therein.

Arguably the most spectacular neutrino phenomenon is oscillation, an effect that goes beyond the SM. Neutrinos come in three flavours: electron, muon and tauon, denoted as $(\nu_e, \nu_\mu, \nu_\tau)$. For neutrinos, the mass and flavour eigenstates differ. The propagation is determined by the mass eigenstates, while their identification is determined by the flavour eigenstates. Neutrinos may change their type with the distance. The simplest model of oscillations was proposed by B. Pontecorvo [4, 5], whereby the neutrino flavour eigenstate is assumed to be a linear combination of its mass eigenstates. The mixing is described by the Pontecorvo–Maki–Nakagawa–Sakata matrix that has several parameters. There have been many experiments aiming to measure these oscillation parameters. Distinguishing only the most popular, we can mention the SNO [6] and Super-Kamiokande [7, 8] experiments working on the solar and atmospheric neutrinos. The Super-Kamiokande detector has also been used in the accelerator experiments K2K [9] and T2K [10]. Other important experiments that use artificial neutrino beams are MiniBooNE [11], MINOS [12], ICARUS [13] and NOvA [14].

Accelerator neutrino beams have wide energy spectra. However, many sources operate mainly in the 1 – 5 GeV energy region. In this low-energy region, the cross section is known with the precision not exceeding 20%. Goals for future experiments, such as DUNE [15] or Hyper-Kamiokande [16], require much greater precision. The most important reaction mechanism within this energy region is the charged current quasielastic scattering (CCQE). For neutrinos and antineutrinos, such a mechanism can be expressed by the following formulae

$$\begin{aligned}\nu_l + n &\rightarrow l^- + p, \\ \bar{\nu}_l + p &\rightarrow l^+ + n,\end{aligned}\tag{1}$$

where $l \in \{e, \mu, \tau\}$, and n and p denote the neutron and proton, respectively.

Important tools that help to validate theoretical models and predict the outcome of the future experiments are Monte Carlo (MC) simulations. In neutrino experiments, one measures not the neutrino itself but the products of its interactions with various atomic nuclei. The main difficulty comes from the fact that one does not know the exact value of the energy of the incident neutrino and, thus, the four-momentum transfer. Hence, a reconstruction procedure is needed. Its accuracy, however, is limited by the theoretical models of the target nucleus. An effective tool for studying the nuclear effects is an electron-nucleus scattering process. Using an electron instead of a neutrino has many advantages. Namely, the experiments are easier to conduct, mainly because the incident electron energy is precisely known; the theoretical description is simplified, but it is done in the same S-matrix perturbative expansion framework. In general, a nuclear model that gives precise results for the electron scattering data is a good foundation for the neutrino case. An electron analogue to the CCQE process is the elastic scattering, where the formulae read

$$\begin{aligned}e^- + p &\rightarrow e^- + p, \\ e^- + n &\rightarrow e^- + n.\end{aligned}\tag{2}$$

Much attention has been brought to the importance of the other final states contributions by the MiniBooNE experiment. The experiment observed an excess of ~ 1 GeV neutrino event rate over the relativistic Fermi Gas (FG) expectation [17]. In order to explain that result, *Martini et al* [18] argued the necessity of including the contribution from the

multi-nucleon emission, especially the emission of two nucleons to the continuum, the so-called 2-particle-2-hole (2p2h) final states. Development of a satisfactory theoretical description of such processes is a complex and demanding task.

Recently, the ArgoNeuT Collaboration reported results from their argon target experiment [19]. The investigation was focused on the sample of neutrino events with no pions and exactly two reconstructed protons in the final state. An effort was made to separate the influence of nucleon correlations, identifying observables that can measure those effects. Although, the ArgoNeuT data are of low statistics and the results are not conclusive, much more data will be soon available from the MicroBooNE experiment [20]. In order to confront the discoveries with theory, we analyzed the data [21, 22] using the NuWro MC event generator [23].

This thesis is organized as follows: in Chapter 1, the cross section of the electron-nucleon scattering is calculated; Chapter 2 contains the analysis of the CCQE electron-nucleus scattering and a brief discussion on the two-body current case; Chapter 3, the final chapter, starts with the discussion on a 2p2h processes. Next the NuWro MC generator and the ArgoNeuT experiment are briefly described. Finally, following ArgoNeuT steps, the discoveries are confronted with the results of the MC simulation.

The purpose of this work is to lay the theoretical foundation for the analysis of the contribution of SRC nucleon-nucleon pairs to the lepton-nucleus scattering problem.

Chapter 1

Electron-nucleon scattering

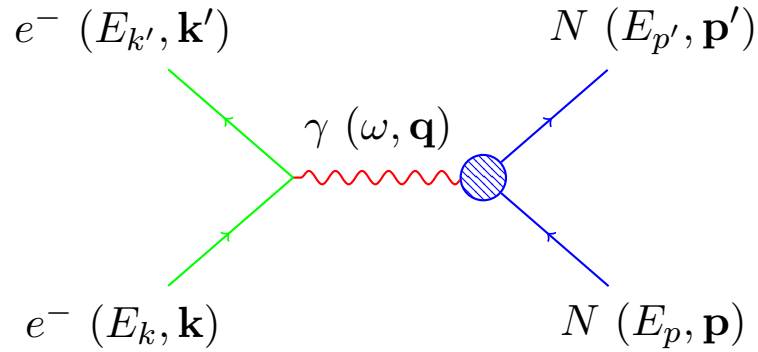


FIGURE 1.1: Feynman diagram for the electron-nucleon scattering in one-photon exchange approximation.

In the quasielastic energy region, the electron-nucleon scattering (2) is an elementary process that can be treated as an introduction to more complex nuclear targets. In this chapter, a detailed analysis of this process is performed. The calculation is patterned mainly on [24] and [25]. The general ideas behind the calculation are introduced in Section 1.1. Then, in Section 1.2, the differential cross section formula, in the language of leptonic ($L_{\mu\nu}$) and hadronic ($W^{\mu\nu}$) tensors, is derived. Section 1.3 contains a discussion on the structure of the hadronic vertex and electromagnetic form factors. The contraction of the leptonic and hadronic tensors, which gives the final result, is presented in Section 1.4. The final section, Section 1.5, is devoted to the interpretation of the results.

1.1 Introduction

Quantum electrodynamics (QED) is the theory used to describe electromagnetic electron-nucleon interaction within the quasielastic energy region. The interaction part of its lagrangian is of the form

$$\mathcal{L}_I = -ej_\mu A^\mu = -e\bar{\psi}\gamma_\mu\psi A^\mu, \quad (1.1)$$

where j^μ is the Dirac current, and A^μ is the virtual photon field. The normalization conventions, including bispinor fermion fields $\psi, \bar{\psi}$, can be found in the appendix [A.3](#).

In the process, all of the particle states are assumed to be plane-waves. The incident electron with four-momentum $k = (E_k, \mathbf{k})$ is scattered through a solid angle $\Omega_{k'}$ to four-momentum $k' = (E_{k'}, \mathbf{k}')$. The four-momenta for the incident and the outgoing nucleons are $p = (E_p, \mathbf{p})$ and $p' = (E_{p'}, \mathbf{p}')$, respectively.

The initial ($|\Psi_i\rangle$) and final ($|\Psi_f\rangle$) states are of the form

$$\begin{aligned} |\Psi_i\rangle &= |\mathbf{k}, s\rangle_e \otimes |\mathbf{p}, r\rangle_N, \\ |\Psi_f\rangle &= |\mathbf{k}', s'\rangle_e \otimes |\mathbf{p}', r'\rangle_N, \end{aligned} \quad (1.2)$$

where s, s', r, r' denote the spins of the particles. The states are defined in the interaction picture.

An important quantity in the qualitative comparison with experimental data is the cross section. A derivation of the general cross section formula can be found in appendix [B.1](#).

The information that is provided by the calculation within Quantum Field Theory (QFT) is the probability of interaction. In the S-matrix formalism, one calculates a matrix element that gives an amplitude of transition between an initial and a final state:

$$P \sim \left| \langle \Psi_f | \hat{S} | \Psi_i \rangle \right|^2. \quad (1.3)$$

The S-matrix in the first order of the perturbation expansion contains a trivial part and the interacting one described by the T-matrix:

$$\hat{S} = 1 + i\hat{T}. \quad (1.4)$$

An important procedure that allows one to properly normalize the wave functions of freely moving particles is the quantization in the finite volume. The cross section is derived for such a regime, and then the infinite volume limit is taken. The detailed description of this procedure can be found in appendix B.2.

1.2 Differential cross section

Nucleons are composite particles. Electron-nucleon scattering can be considered as a scattering of an electron off the four-potential $A^\mu(x)$ generated by the hadronic current $\mathcal{J}^\mu(x)$. Using Maxwell equations, one has

$$\square A^\mu(x) = -e \mathcal{J}^\mu(x). \quad (1.5)$$

An essential part of the cross section calculation is the T-matrix element. An easy way to identify its components is by utilizing the language of Feynman rules, see the appendix B.3. In the Fig. 1.1, the lowest order Feynman diagram for the process is presented.

Using Feynman rules, for every vertex a factor of $-ie j_\mu(x)$, integrated over all possible x , is taken. For the hadronic vertex, the Dirac current $j_\mu(x)$ needs to be substituted with the hadronic current $\mathcal{J}_\mu(x)$. Additionally, one needs to include a virtual photon propagator and integrate it over all possible four-momentum transfers q . Hence, including additional numeric factors, the T-matrix element, in the one-photon exchange approximation, is of the form

$$\begin{aligned} \langle \Psi_f | i\hat{T} | \Psi_i \rangle &= -i \int \frac{d^4q}{(2\pi)^4} \left(\frac{-ig^{\mu\nu}}{q^2} \right) \\ &\times \left(-ie \left\langle \mathbf{k}', s' \left| \int_{\Omega} d^4x e^{-iq \cdot x} j_\mu(x) \right| \mathbf{k}, s \right\rangle \right) \\ &\times \left(-ie \left\langle \mathbf{p}', r' \left| \int_{\Omega} d^4y e^{iq \cdot y} \mathcal{J}_\nu(y) \right| \mathbf{p}, r \right\rangle \right), \end{aligned} \quad (1.6)$$

where $\Omega = V \cdot T$ is the volume in the Minkowski space. This formula can be further simplified, and one obtains

$$\begin{aligned} \langle \Psi_f | i\hat{T} | \Psi_i \rangle &= \int \frac{d^4q}{(2\pi)^4} \frac{e^2}{q^2} \\ &\times \int_{\Omega} d^4x e^{-iq \cdot x} \langle \mathbf{k}', s' | j_{\mu}(x) | \mathbf{k}, s \rangle \int_{\Omega} d^4y e^{iq \cdot y} \langle \mathbf{p}', r' | \mathcal{J}^{\mu}(y) | \mathbf{p}, r \rangle. \end{aligned} \quad (1.7)$$

As all of the particles are on-shell, the one-particle states can be easily chosen to be the eigenstates of four-momentum. Time evolutions of the probability currents are given by

$$\begin{aligned} j_{\mu}(x^0, \mathbf{x}) &= e^{-i\hat{H}x^0} j_{\mu}(0, \mathbf{x}) e^{i\hat{H}x^0}, \\ \mathcal{J}^{\mu}(y^0, \mathbf{y}) &= e^{-i\hat{H}y^0} \mathcal{J}^{\mu}(0, \mathbf{y}) e^{i\hat{H}y^0}. \end{aligned} \quad (1.8)$$

On the other hand, the translations read

$$\begin{aligned} j_{\mu}(x^0, \mathbf{x}) &= e^{i\hat{P} \cdot \mathbf{x}} j_{\mu}(x^0, 0) e^{-i\hat{P} \cdot \mathbf{x}}, \\ \mathcal{J}^{\mu}(y^0, \mathbf{y}) &= e^{i\hat{P} \cdot \mathbf{y}} \mathcal{J}^{\mu}(y^0, 0) e^{-i\hat{P} \cdot \mathbf{y}}. \end{aligned} \quad (1.9)$$

Using (1.8,1.9) and the fact that the states are the four-momentum eigenstates, the current's spacetime dependence can be cleared. First, for the time dependence, one obtains

$$\begin{aligned} \langle \Psi_f | i\hat{T} | \Psi_i \rangle &= \int \frac{d^4q}{(2\pi)^4} \frac{e^2}{q^2} \\ &\times \int_{\Omega} d^4x e^{-iq \cdot x} \langle \mathbf{k}', s' | e^{-i\hat{H}x^0} j_{\mu}(0, \mathbf{x}) e^{i\hat{H}x^0} | \mathbf{k}, s \rangle \\ &\times \int_{\Omega} d^4y e^{iq \cdot y} \langle \mathbf{p}', r' | e^{-i\hat{H}y^0} \mathcal{J}_{\mu}(0, \mathbf{y}) e^{i\hat{H}y^0} | \mathbf{p}, r \rangle \\ &= \int \frac{d^4q}{(2\pi)^4} \frac{e^2}{q^2} \\ &\times \int_{\Omega} d^4x e^{-iq \cdot x} \langle \mathbf{k}', s' | e^{-iE_{k'}x^0} j_{\mu}(0, \mathbf{x}) e^{iE_kx^0} | \mathbf{k}, s \rangle \\ &\times \int_{\Omega} d^4y e^{iq \cdot y} \langle \mathbf{p}', r' | e^{-iE_{p'}y^0} \mathcal{J}_{\mu}(0, \mathbf{y}) e^{iE_p y^0} | \mathbf{p}, r \rangle \\ &= \int \frac{d^4q}{(2\pi)^4} \frac{e^2}{q^2} \\ &\times \int_{\Omega} d^4x e^{-i(\omega + E_{k'} - E_k)x^0} e^{i\mathbf{q} \cdot \mathbf{x}} \langle \mathbf{k}', s' | j_{\mu}(0, \mathbf{x}) | \mathbf{k}, s \rangle \\ &\times \int_{\Omega} d^4y e^{i(\omega - E_{p'} + E_p)y^0} e^{-i\mathbf{q} \cdot \mathbf{y}} \langle \mathbf{p}', r' | \mathcal{J}_{\mu}(0, \mathbf{y}) | \mathbf{p}, r \rangle. \end{aligned} \quad (1.10)$$

Then, for the spacial dependence, one obtains

$$\begin{aligned}
\langle \Psi_f | i\hat{T} | \Psi_i \rangle &= \int \frac{d^4q}{(2\pi)^4} \frac{e^2}{q^2} \\
&\times \int_{\Omega} d^4x e^{-i(\omega+E_{k'}-E_k)x^0} e^{i\mathbf{q}\cdot\mathbf{x}} \langle \mathbf{k}', s' | e^{i\hat{P}\cdot\mathbf{x}} j_{\mu}(0) e^{-i\hat{P}\cdot\mathbf{x}} | \mathbf{k}, s \rangle \\
&\times \int_{\Omega} d^4y e^{i(\omega-E_{p'}+E_p)y^0} e^{-i\mathbf{q}\cdot\mathbf{y}} \langle \mathbf{p}', r' | e^{i\hat{P}\cdot\mathbf{y}} \mathcal{J}^{\mu}(0) e^{-i\hat{P}\cdot\mathbf{y}} | \mathbf{p}, r \rangle \\
&= \int \frac{d^4q}{(2\pi)^4} \frac{e^2}{q^2} \\
&\times \int_{\Omega} d^4x e^{-i(\omega+E_{k'}-E_k)x^0} e^{i\mathbf{q}\cdot\mathbf{x}} \langle \mathbf{k}', s' | e^{i\mathbf{k}'\cdot\mathbf{x}} j_{\mu}(0) e^{-i\mathbf{k}\cdot\mathbf{x}} | \mathbf{k}, s \rangle \quad (1.11) \\
&\times \int_{\Omega} d^4y e^{i(\omega-E_{p'}+E_p)y^0} e^{-i\mathbf{q}\cdot\mathbf{y}} \langle \mathbf{p}', r' | e^{i\mathbf{p}'\cdot\mathbf{y}} \mathcal{J}^{\mu}(0) e^{-i\mathbf{p}\cdot\mathbf{y}} | \mathbf{p}, r \rangle \\
&= \int \frac{d^4q}{(2\pi)^4} \frac{e^2}{q^2} \\
&\times \int_{\Omega} d^4x e^{-i(q+k'-k)\cdot x} \langle \mathbf{k}', s' | j_{\mu}(0) | \mathbf{k}, s \rangle \\
&\times \int_{\Omega} d^4y e^{i(q-p'+p)\cdot y} \langle \mathbf{p}', r' | \mathcal{J}^{\mu}(0) | \mathbf{p}, r \rangle.
\end{aligned}$$

The next step is to perform the integrations over d^4x and d^4y . As the integrals are constrained by the finite volume, a special treatment must be applied. A detailed discussion about the properties of the Dirac deltas in finite volume can be found in appendix B.2. By integrating over, one gets

$$\begin{aligned}
\langle \Psi_f | i\hat{T} | \Psi_i \rangle &= \int \frac{d^4q}{(2\pi)^4} \frac{e^2}{q^2} \\
&\times (2\pi)^4 \delta_{\Omega}^{(4)}(q+k'-k) \langle \mathbf{k}', s' | j_{\mu}(0) | \mathbf{k}, s \rangle \\
&\times (2\pi)^4 \delta_{\Omega}^{(4)}(q-p'+p) \langle \mathbf{p}', r' | \mathcal{J}^{\mu}(0) | \mathbf{p}, r \rangle \quad (1.12) \\
&= (2\pi)^4 \frac{e^2}{q^2} \delta_{\Omega}^{(4)}(k-k'-p'+p) \\
&\times \langle \mathbf{k}', s' | j_{\mu}(0) | \mathbf{k}, s \rangle \langle \mathbf{p}', r' | \mathcal{J}^{\mu}(0) | \mathbf{p}, r \rangle.
\end{aligned}$$

As shown in the appendix B.2, the differential cross section formula for this process is of the form

$$d\sigma = \frac{1}{2E_k 2E_p} \frac{d^3\mathbf{k}'}{2(2\pi)^3 E_{k'}} \frac{d^3\mathbf{p}'}{2(2\pi)^3 E_{p'}} \frac{1}{\nu} \frac{1}{\Omega} \left| \langle \Psi_f | i\hat{T} | \Psi_i \rangle \right|^2. \quad (1.13)$$

The electrons are considered to be relativistic, hence $\nu = \frac{|\mathbf{k}|}{E_k} \simeq 1$.

The problematic point in squaring the T-matrix element is the square of the Dirac delta. However, using (B.20) this difficulty can be overcome, and one can obtain the sixfold

differential cross section formula of the form

$$\frac{d\sigma}{d^3\mathbf{k}'d^3\mathbf{p}'} = \frac{1}{4} \frac{1}{E_k E_p E_{k'} E_{p'}} \frac{\alpha^2}{q^4} L_{\mu\nu} W^{\mu\nu}, \quad (1.14)$$

where the following structures have been used:

- the leptonic tensor:

$$L_{\mu\nu} \equiv \frac{1}{2} \sum_{s,s'} \langle \mathbf{k}', s' | j_\mu(0) | \mathbf{k}, s \rangle \langle \mathbf{k}', s' | j_\nu(0) | \mathbf{k}, s \rangle^*, \quad (1.15)$$

- the hadronic tensor:

$$W^{\mu\nu} = \frac{1}{2} \sum_{r,r'} \langle \mathbf{p}', r' | \mathcal{J}^\mu(0) | \mathbf{p}, r \rangle \langle \mathbf{p}', r' | \mathcal{J}^\nu(0) | \mathbf{p}, r \rangle^* \delta^{(4)}(p' - p - q) \Big|_{q=k-k'}. \quad (1.16)$$

Note that the spins of particles are assumed to be not measured and the additional average over the spins have to be included.

As shown in appendix C.1, using the Dirac delta function from the hadronic tensor (1.16), one can perform an integration over the four dimensions and obtain the twofold differential cross section formula

$$\frac{d\sigma}{d\Omega_{k'}} = \frac{1}{4} \frac{E_{k'}^2}{E_k^2} \frac{1}{E_p^2} \frac{\alpha^2}{q^4} L_{\mu\nu} H^{\mu\nu}, \quad (1.17)$$

where

$$W^{\mu\nu} = H^{\mu\nu} \delta^{(4)}(p' - p - q). \quad (1.18)$$

1.3 Electromagnetic form factors

Electrons are point-like particles thus the leptonic current is given by (1.1). The current has been already taken without any spacetime dependence; using (A.27), one obtains

$$\langle \mathbf{k}', s' | j_\mu(0) | \mathbf{k}, s \rangle = \bar{u}(\mathbf{k}', s') \gamma_\mu u(\mathbf{k}, s). \quad (1.19)$$

However, nucleons need special attention. They are composite particles and cannot be treated as point-like. An important feature is the fact that the magnetic moments of

nucleons differ from the Dirac one ($e/2M$). The differences are by a factor of ~ 2.79 and ~ -1.91 , for protons and neutrons respectively [26]. In general, nucleons are coupled with various virtual particles, especially with mesons. As the structure of such impact might be very complex, an effective mechanism needs to be used.

The strategy here is to introduce an effective vertex Γ^μ [27]. The number of its components can be constrained demanding the Lorentz invariance. It can be built using hadronic four-momenta (p^μ, p'^μ), nucleon mass M , and matrices: $\{\mathbb{1}, \gamma^\mu, \sigma^{\mu\nu}\}$. As only electromagnetic interactions are considered, the γ_5 matrix cannot be used. The particles are on-shell. Therefore, the Dirac equation provides an additional constraint. The Γ^μ vertex is taken up to the scalar coefficients called the form factors. The only scalar that can be built using the hadronic four-momenta p^μ and p'^μ is the product $p_\mu p'^\mu$, which can be expressed by the squared four-momentum transfer q^2 . Therefore form factors $F_{1,2}$ are the functions of q^2 . Proceeding analogous to (1.19), one obtains

$$\langle \mathbf{p}', r' | \mathcal{J}^\mu(0) | \mathbf{p}, r \rangle = \bar{u}(\mathbf{p}', r') \Gamma^\mu(q^2) u(\mathbf{p}, r), \quad (1.20)$$

where

$$\Gamma^\mu(q^2) = \gamma^\mu F_1(q^2) + \frac{i}{2M} \sigma^{\mu\alpha} q_\alpha F_2(q^2). \quad (1.21)$$

Note that protons and neutrons have different form factors, $F_{1,2}$.

1.4 Tensor contraction

Using (1.19), the leptonic tensor can be expressed as

$$L_{\mu\nu} = \frac{1}{2} \sum_{s,s'} (\bar{u}(\mathbf{k}', s') \gamma_\mu u(\mathbf{k}, s)) (\bar{u}(\mathbf{k}', s') \gamma_\nu u(\mathbf{k}, s))^*. \quad (1.22)$$

As shown in appendix C.2, the summation over spins can be done, and the leptonic tensor can be rewritten as

$$L_{\mu\nu} = 2(k'_\mu k_\nu + k'_\nu k_\mu - g_{\mu\nu} k' \cdot k). \quad (1.23)$$

On the other hand, using (1.20), the hadronic tensor can be expressed as

$$H^{\mu\nu} = \frac{1}{2} \sum_{s,s'} \bar{u}(\mathbf{p}', s') \Gamma^\mu u(\mathbf{p}, s) (\bar{u}(\mathbf{p}', s') \Gamma^\nu u(\mathbf{p}, s))^*. \quad (1.24)$$

Again, the summation over spins can be calculated, the details can be found in the appendix C.3. The hadronic tensor reads

$$H^{\mu\nu} = \left[(F_1 + F_2)^2 q^2 \left(g^{\mu\nu} - \frac{q^\mu q^\nu}{q^2} \right) + \left(F_1^2 - \frac{q^2}{4M^2} F_2^2 \right) (q + 2p)^\mu (q + 2p)^\nu \right]. \quad (1.25)$$

Now, one can contract the leptonic and hadronic tensors. As shown in the appendix C.4, one obtains

$$L_{\mu\nu} H^{\mu\nu} = 2(F_1 + F_2)^2 q^4 + 8 \left(F_1^2 - \frac{q^2}{4M^2} F_2^2 \right) \left[2(k' \cdot p)(k \cdot p) + \frac{q^2}{2} M^2 \right]. \quad (1.26)$$

It is convenient to choose a specific frame of reference that can simplify the results. A common choice is the target nucleon rest-frame, where $E_p = M$. Here, the contraction reads

$$\begin{aligned} L_{\mu\nu} H^{\mu\nu} &= 2(F_1 + F_2)^2 q^2 q^2 + 8 \left(F_1^2 - \frac{q^2}{4M^2} F_2^2 \right) \left[2E_k E_{k'} M^2 + \frac{q^2}{2} M^2 \right] \\ &= -8(F_1 + F_2)^2 q^2 E_k E_{k'} \sin^2 \frac{\theta}{2} \\ &\quad + 8 \left(F_1^2 - \frac{q^2}{4M^2} F_2^2 \right) \left[2E_{k'} E_k M^2 - 2E_k E_{k'} M^2 \sin^2 \frac{\theta}{2} \right] \\ &= 16E_k E_{k'} M^2 \cos^2 \frac{\theta}{2} \left[-\frac{q^2}{2M^2} \text{tg}^2 \frac{\theta}{2} (F_1 + F_2)^2 + \left(F_1^2 - \frac{q^2}{4M^2} F_2^2 \right) \right] \end{aligned} \quad (1.27)$$

The contraction can be put into the formula (1.17) to obtain the final result,

$$\frac{d\sigma}{d\Omega_{k'}} = \frac{\alpha^2 \cos^2 \frac{\theta}{2} E_{k'}}{4 \sin^4 \frac{\theta}{2} E_k^3} \left[\left(F_1^2 - \frac{q^2}{4M^2} F_2^2 \right) - (F_1 + F_2)^2 \frac{q^2}{2M^2} \text{tg}^2 \frac{\theta}{2} \right]. \quad (1.28)$$

Take note that Eq. (1.26) will be useful in the next chapter, where the target nucleon rest-frame cannot be chosen.

1.5 Interpretation

The cross section formula can be rewritten in the compact form

$$\frac{d\sigma}{d\Omega_{k'}} = \left(\frac{d\sigma}{d\Omega_{k'}} \right)_{\text{Mott}} \left[\left(F_1^2 - \frac{q^2}{4M^2} F_2^2 \right) - (F_1 + F_2)^2 \frac{q^2}{2M^2} \text{tg}^2 \frac{\theta}{2} \right], \quad (1.29)$$

where

$$\left(\frac{d\sigma}{d\Omega_{k'}} \right)_{\text{Mott}} = \frac{\alpha^2 E_{k'} \cos^2 \frac{\theta}{2}}{4E_k^3 \sin^4 \frac{\theta}{2}} \quad (1.30)$$

is the Mott cross section: the formula for an electron scattering off the positively charged point in space.

Note that taking the form factors $F_1 = 1$ and $F_2 = 0$ in (1.21), one restores the formula for the electron scattering on the point-like proton.

Moreover, a different approach can be taken. The hadronic tensor $H^{\mu\nu}$ can be written in the most general Lorentz and gauge invariant form [24],

$$H^{\mu\nu} = H_1 \left(\frac{q^\mu q^\nu}{q^2} - g^{\mu\nu} \right) + \frac{H_2}{M^2} \left(p^\mu - q^\mu \frac{p \cdot q}{q^2} \right) \left(p^\nu - q^\nu \frac{p \cdot q}{q^2} \right). \quad (1.31)$$

Then, comparing it with (1.25), one can identify

$$\begin{aligned} H_1 &= -(F_1 + F_2)^2 q^2 \\ H_2 &= 4 \left(M^2 F_1^2 - \frac{q^2}{4} F_2^2 \right), \end{aligned} \quad (1.32)$$

and write

$$\frac{d\sigma}{d\Omega_{k'}} = \left(\frac{d\sigma}{d\Omega_{k'}} \right)_{\text{Mott}} \frac{1}{4M^2} \left[2H_1 \text{tg}^2 \frac{\theta}{2} + H_2 \right]. \quad (1.33)$$

Although, the role of F_1, F_2 is clear on the level of an effective Γ^μ vertex, their interpretation in the context of the cross section formula is not trivial. In experiments, ather set of form factors is often used. The so-called Sachs form factors G_E, G_M in the Breit frame of reference have an interpretation of measuring the charge and magnetization distribution respectively [28]. They are given by

$$\begin{aligned} G_E(q^2) &= F_1(q^2) + \tau F_2(q^2), \\ G_M(q^2) &= F_1(q^2) + F_2(q^2), \end{aligned} \quad (1.34)$$

where the parameter $\tau = -\frac{q^2}{4M^2}$. The reverse relations read

$$\begin{aligned} F_1(q^2) &= \frac{G_E(q^2) + \tau G_M(q^2)}{1 + \tau}, \\ F_2(q^2) &= \frac{G_M(q^2) - G_E(q^2)}{1 + \tau}. \end{aligned} \quad (1.35)$$

In the new parametrization, the cross section formula is given by

$$\frac{d\sigma}{d\Omega_{k'}} = \left(\frac{d\sigma}{d\Omega_{k'}} \right)_{\text{Mott}} \left[\frac{G_E^2 + \tau G_M^2 \left(1 + 2(1 + \tau) \text{tg}^2 \frac{\theta}{2} \right)}{1 + \tau} \right]. \quad (1.36)$$

One can introduce the virtual photon polarization $\epsilon = \left(1 + 2(1 + \tau) \text{tg}^2 \frac{\theta}{2} \right)^{-1}$. Then, one can consider the reduced cross section

$$\left(\frac{d\sigma}{d\Omega_{k'}} \right)_{\text{red}} \equiv \frac{\epsilon(1 + \tau)}{\tau} \left(\frac{d\sigma}{d\Omega_{k'}} \right) / \left(\frac{d\sigma}{d\Omega_{k'}} \right)_{\text{Mott}} = \frac{\epsilon}{\tau} G_E^2 + G_M^2. \quad (1.37)$$

With experimental data for the measured reduced cross section, one obtains form factors G_E^2, G_M^2 from the linear fit.

As the factors G_E, G_M are the Fourier transforms of the charge distribution and the magnetic moment, respectively, one can assume the dipole approximation and introduce the dipole form factor

$$G_D(q^2) \equiv \left(1 + \frac{q^2}{M_V^2} \right)^{-2} = \left(1 - \frac{q^2}{0.71 \text{GeV}^2} \right)^{-2}, \quad (1.38)$$

where $M_V = 0.84 \text{GeV}$. The proton form factors are given by

$$\begin{aligned} G_E^p(q^2) &= G_D(q^2), \\ G_M^p(q^2) &= \mu_p G_D(q^2), \end{aligned} \quad (1.39)$$

and for the neutron

$$\begin{aligned} G_E^n(q^2) &= 0, \\ G_M^n(q^2) &= \mu_n G_D(q^2), \end{aligned} \quad (1.40)$$

where the magnetic form factors G_M are assumed to have the same q^2 dependency as the G_E , and the magnetic moments read $\mu_p = 2.7928$ and $\mu_n = -1.9130$ in the units of nuclear magnetons [26].

Note that for $q^2 = 0$ the form factors are of the form

$$\begin{aligned} F_1^p(0) &= 1, \\ F_2^p(0) &= \mu_p - 1, \\ F_1^n(0) &= 0, \\ F_2^n(0) &= \mu_n. \end{aligned} \tag{1.41}$$

For a review on the recent measurements of the nucleon form factors see, e.g., [29].

Chapter 2

Electron-nucleus scattering

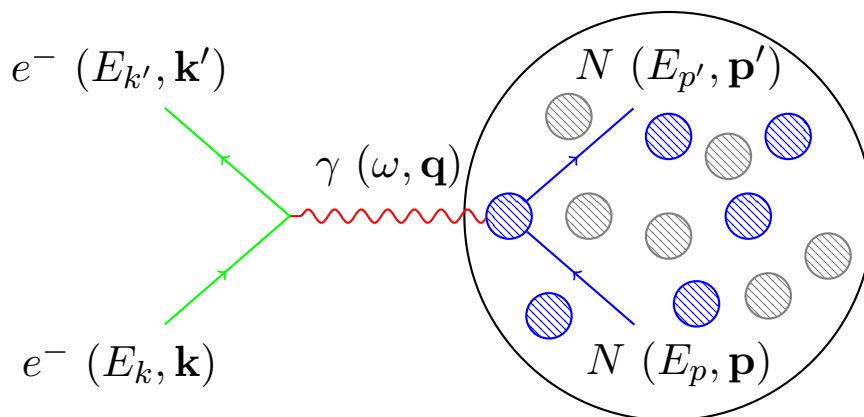


FIGURE 2.1: Feynman diagram for the electron-nucleus scattering in the impulse approximation.

The nucleus is a quantum many-body system, and it is not obvious how such a system should be described. Many approximations have to be made, leaving the essential task to analyze their significance in a chosen energy region. The quasielastic lepton-nucleus is commonly described using the *plane wave impulse approximation* (PWIA), where the cross section can be factorized [30], i.e., expressed by the elementary lepton-nucleon cross section multiplied by the spectral function (SF). This function can be interpreted as the probability of finding, inside the nuclear target, a nucleon of specific momentum that leaves the residual system with a given excitation energy [31]. Hence, it contains information about the structure and the dynamics of the nucleus.

In this chapter, a detailed analysis of the elastic electron-nucleus interaction is performed. In Section 2.1, the problem is briefly introduced, emphasising the differences against the electron-nucleon process. Then, in Section 2.2, the impulse approximation is

presented. Section 2.3 contains a discussion about the plane wave impulse approximation: the formalism, the factorization properties, and the calculation for a given nucleon within the target nucleus. Finally, in Section 2.4, the analysis is complemented with the relativistic plane wave impulse approximation, i.e., the calculation that assumes a bound relativistic nucleon.

2.1 Introduction

Since the result is derived on the level of QED, the foundation for the calculation of the electron-nucleus scattering is similar to the electron-nucleon process. However, the free nucleon states need to be replaced with composite nuclear states. The initial (I) and the final (F) hadronic states have four-momenta $p_I = (E_I, \mathbf{p}_I)$ and $p_F = (E_F, \mathbf{p}_F)$, respectively. For the hadronic states, the following notation is used: $|X, \mathbf{p}_X\rangle$ is a state of four-momentum $p_X = (E_X, \mathbf{p}_X)$; the letter X contains the quantum numbers (spin σ_X , isospin τ_X) and fully characterizes the hadronic state. The initial (Ψ_i) and final (Ψ_f) states for the whole process can be written as

$$\begin{aligned} |\Psi_i\rangle &= |\mathbf{k}, s\rangle_e \otimes |I, \mathbf{p}_I\rangle_A \\ |\Psi_f\rangle &= |\mathbf{k}', s'\rangle_e \otimes |F, \mathbf{p}_F\rangle_A, \end{aligned} \quad (2.1)$$

where the initial hadronic state is a given nuclear groundstate of atomic number A , and the final hadronic state is arbitrary.

The T-matrix element for this process is analogous to (1.7), and the same calculation for the currents spacetime dependence as in (1.10, 1.11) can be performed. However, the hadronic states are not assumed to be the four-momentum eigenstates. At this point, one takes the energy eigenstates and still clear the time dependence of the hadronic current. The T-matrix element reads

$$\begin{aligned} \langle \Psi_f | i\hat{T} | \Psi_i \rangle &= \int d^4q \frac{e^2}{q^2} \delta_\Omega^{(4)}(q + k' - k) \bar{u}(\mathbf{k}', s') \gamma_\mu u(\mathbf{k}, s) \\ &\times (2\pi) \delta_T(E_F - E_I + \omega) \left\langle F, \mathbf{p}_F \left| \int_V d^3\mathbf{x} e^{-i\mathbf{q}\cdot\mathbf{x}} \mathcal{J}^\mu(\mathbf{x}) \right| I, \mathbf{p}_I \right\rangle. \end{aligned} \quad (2.2)$$

Similarly to (1.14), one can use the results from appendix B.2 to obtain

$$\frac{d\sigma_F}{d^3\mathbf{k}'d^3\mathbf{p}_F} = \frac{1}{4} \frac{1}{E_k E_I E_{k'} E_F} \frac{\alpha^2}{q^4} L_{\mu\nu} W^{\mu\nu}, \quad (2.3)$$

where the leptonic tensor is given by (1.15), but the hadronic tensor reads

$$\begin{aligned} W^{\mu\nu} &= \sum_{\sigma_I} \left\langle F, \mathbf{p}_F \left| \int_V d^3\mathbf{x} e^{-i\mathbf{q}\cdot\mathbf{x}} \mathcal{J}^\mu(\mathbf{x}) \right| I, \mathbf{p}_I \right\rangle \left\langle I, \mathbf{p}_I \left| \int_V d^3\mathbf{x} e^{i\mathbf{q}\cdot\mathbf{x}} \mathcal{J}^{\nu\dagger}(\mathbf{x}) \right| F, \mathbf{p}_F \right\rangle \\ &\times \frac{1}{(2\pi)^3 V} \delta(E_F - E_I - \omega) \Big|_{q=k-k'}. \end{aligned} \quad (2.4)$$

Including factor $((2\pi)^3 V)^{-1}$ in the hadronic tensor keeps the cross section in a form analogous to the electron-nucleon case. Note that one needs to sum over all possible spins of the initial state I .

The inclusive cross section, that takes into account all possible final states, reads

$$d\sigma = \sum_F d\sigma_F. \quad (2.5)$$

In the electron-nucleus interaction process, the nontrivial part is the nuclear response. Here, it is enclosed in the hadronic tensor. For the inclusive process, with the summation over final states F and the integration over $d^3\mathbf{p}_F$ included, the hadronic tensor reads

$$\begin{aligned} W^{\mu\nu} &= \sum_{F, \sigma_I} \int d^3\mathbf{p}_F \left\langle F, \mathbf{p}_F \left| \int_V d^3\mathbf{x} e^{-i\mathbf{q}\cdot\mathbf{x}} \mathcal{J}^\mu(\mathbf{x}) \right| I, \mathbf{p}_I \right\rangle \left\langle I, \mathbf{p}_I \left| \int_V d^3\mathbf{x} e^{i\mathbf{q}\cdot\mathbf{x}} \mathcal{J}^{\nu\dagger}(\mathbf{x}) \right| F, \mathbf{p}_F \right\rangle \\ &\times \frac{1}{(2\pi)^3 V} \delta(E_F - E_I - \omega) \Big|_{q=k-k'}. \end{aligned} \quad (2.6)$$

The following discussion will be held in the initial nucleus rest-frame, where $p_I = (M_A, \mathbf{0})$.

2.2 Impulse Approximation

A virtual photon of momentum \mathbf{q} can probe the distances of the order of $1/|\mathbf{q}|$. For sufficiently high momentum transfers ($|\mathbf{q}| > 400$ MeV) [32], one can use the *impulse*

approximation. This procedure treats interactions with different nucleons within the nucleus separately. The scheme of this process is presented in Fig. 2.1.

2.2.1 One-body current

The probability of an interaction with the nucleus is given by the incoherent sum over the probabilities of interacting with each of the nucleons. This scheme is equivalent to taking the sum of one-body interactions over all nonrelativistic nucleons. In the second quantization language, the one-body current reads

$$\begin{aligned} \mathcal{J}^\mu(\mathbf{x}) \approx & \sum_{N=p,n}^A \sum_{\sigma_{N'}} \int \frac{d^3\mathbf{p}_{N'}}{(2\pi)^3\sqrt{2E_{N'}}} \frac{d^3\mathbf{p}_N}{(2\pi)^3\sqrt{2E_N}} \langle N', \mathbf{p}_{N'} | j^\mu(\mathbf{x}) | N, \mathbf{p}_N \rangle \\ & \times a_{N'}^\dagger(\mathbf{p}_{N'}) a_N(\mathbf{p}_N) \Big|_{\tau_N=\tau_{N'}}, \end{aligned} \quad (2.7)$$

where we take under consideration all possible nucleon (N) extraction out of the initial nucleus. As only the elastic process is considered, both N and N' must be the same particles: protons or neutrons. In other words, the isospin in this process is conserved and the summation over N' is only a summation over spins. The factors $((2\pi)^3\sqrt{2E})^{-1}$ account for the normalization convention (A.26). The one-body current conjugation operator is of the form

$$\begin{aligned} \mathcal{J}^{\nu\dagger}(\mathbf{x}) \approx & \sum_{M=p,n}^A \sum_{\sigma_{M'}} \int \frac{d^3\mathbf{p}_{M'}}{(2\pi)^3\sqrt{2E_{M'}}} \frac{d^3\mathbf{p}_M}{(2\pi)^3\sqrt{2E_M}} \langle M, \mathbf{p}_M | j^{\nu\dagger}(\mathbf{x}) | M', \mathbf{p}_{M'} \rangle \\ & \times a_M^\dagger(\mathbf{p}_M) a_{M'}(\mathbf{p}_{M'}) \Big|_{\tau_M=\tau_{M'}}. \end{aligned} \quad (2.8)$$

2.2.2 Hadronic tensor

In order to express the hadronic tensor (2.6) in the impulse approximation, one needs to calculate the current matrix elements first. Here, the one-particle states (N, N', M, M') are assumed to be the momentum eigenstates. The same procedure of clearing the current space dependence (1.11) can be performed. Then, the current matrix elements

are then given by

$$\begin{aligned}
& \left\langle F, \mathbf{p}_F \left| \int_V d^3\mathbf{x} e^{-i\mathbf{q}\cdot\mathbf{x}} \mathcal{J}^\mu(\mathbf{x}) \right| I \right\rangle = \\
& = \left\langle F, \mathbf{p}_F \left| \int_V d^3\mathbf{x} e^{-i\mathbf{q}\cdot\mathbf{x}} \right. \right. \\
& \times \left. \left(\sum_{N=p,n}^A \sum_{\sigma_{N'}} \int \frac{d^3\mathbf{p}_{N'}}{(2\pi)^3 \sqrt{2E_{N'}}} \frac{d^3\mathbf{p}_N}{(2\pi)^3 \sqrt{2E_N}} \langle N', \mathbf{p}_{N'} | j^\mu(\mathbf{x}) | N, \mathbf{p}_N \rangle a_{N'}^\dagger(\mathbf{p}_{N'}) a_N(\mathbf{p}_N) \right) \right| I \rangle \\
& = \int_V d^3\mathbf{x} e^{-i\mathbf{q}\cdot\mathbf{x}} \sum_{N=p,n}^A \sum_{\sigma_{N'}} \int \frac{d^3\mathbf{p}_{N'}}{(2\pi)^3 \sqrt{2E_{N'}}} \frac{d^3\mathbf{p}_N}{(2\pi)^3 \sqrt{2E_N}} \\
& \times \langle N', \mathbf{p}_{N'} | j^\mu(\mathbf{x}) | N, \mathbf{p}_N \rangle \left\langle F, \mathbf{p}_F \left| a_{N'}^\dagger(\mathbf{p}_{N'}) a_N(\mathbf{p}_N) \right| I \right\rangle \\
& = (2\pi)^3 \sum_{N=p,n}^A \sum_{\sigma_{N'}} \int \frac{d^3\mathbf{p}_{N'}}{(2\pi)^3 \sqrt{2E_{N'}}} \frac{d^3\mathbf{p}_N}{(2\pi)^3 \sqrt{2E_N}} \delta_V^{(3)}(\mathbf{p}_{N'} - \mathbf{p}_N - \mathbf{q}) \\
& \times \langle N', \mathbf{p}_{N'} | j^\mu(0) | N, \mathbf{p}_N \rangle \left\langle F, \mathbf{p}_F \left| a_{N'}^\dagger(\mathbf{p}_{N'}) a_N(\mathbf{p}_N) \right| I \right\rangle,
\end{aligned} \tag{2.9}$$

and

$$\begin{aligned}
& \left\langle I \left| \int_V d^3\mathbf{x} e^{i\mathbf{q}\cdot\mathbf{x}} \mathcal{J}^{\nu\dagger}(\mathbf{x}) \right| F, \mathbf{p}_F \right\rangle = \\
& = \left\langle I \left| \int_V d^3\mathbf{x} e^{i\mathbf{q}\cdot\mathbf{x}} \right. \right. \\
& \times \left. \left(\sum_{M=p,n}^A \sum_{\sigma_{M'}} \int \frac{d^3\mathbf{p}_{M'}}{(2\pi)^3 \sqrt{2E_{M'}}} \frac{d^3\mathbf{p}_M}{(2\pi)^3 \sqrt{2E_M}} \langle M, \mathbf{p}_M | j^{\nu\dagger}(\mathbf{x}) | M', \mathbf{p}_{M'} \rangle a_M^\dagger(\mathbf{p}_M) a_{M'}(\mathbf{p}_{M'}) \right) \right| F, \mathbf{p}_F \rangle \\
& = \int_V d^3\mathbf{x} e^{i\mathbf{q}\cdot\mathbf{x}} \sum_{M=p,n}^A \sum_{\sigma_{M'}} \int \frac{d^3\mathbf{p}_{M'}}{(2\pi)^3 \sqrt{2E_{M'}}} \frac{d^3\mathbf{p}_M}{(2\pi)^3 \sqrt{2E_M}} \\
& \times \langle M, \mathbf{p}_M | j^{\nu\dagger}(\mathbf{x}) | M', \mathbf{p}_{M'} \rangle \left\langle I \left| a_M^\dagger(\mathbf{p}_M) a_{M'}(\mathbf{p}_{M'}) \right| F, \mathbf{p}_F \right\rangle \\
& = (2\pi)^3 \sum_{M=p,n}^A \sum_{\sigma_{M'}} \int \frac{d^3\mathbf{p}_{M'}}{(2\pi)^3 \sqrt{2E_{M'}}} \frac{d^3\mathbf{p}_M}{(2\pi)^3 \sqrt{2E_M}} \delta_V^{(3)}(\mathbf{p}_M - \mathbf{p}_{M'} + \mathbf{q}) \\
& \times \langle M, \mathbf{p}_M | j^{\nu\dagger}(0) | M', \mathbf{p}_{M'} \rangle \left\langle I \left| a_M^\dagger(\mathbf{p}_M) a_{M'}(\mathbf{p}_{M'}) \right| F, \mathbf{p}_F \right\rangle.
\end{aligned} \tag{2.10}$$

Combining the results, one obtains

$$\begin{aligned}
W^{\mu\nu} &= \sum_{F,\sigma_I} \int d^3\mathbf{p}_F \frac{(2\pi)^3}{V} \delta(E_F - M_A - \omega) \\
&\times \sum_{N=p,n}^A \sum_{\sigma_{N'}} \int \frac{d^3\mathbf{p}_{N'}}{(2\pi)^3 \sqrt{2E_{N'}}} \frac{d^3\mathbf{p}_N}{(2\pi)^3 \sqrt{2E_N}} \delta_V^{(3)}(\mathbf{p}_{N'} - \mathbf{p}_N - \mathbf{q}) \\
&\times \langle N', \mathbf{p}_{N'} | j^\mu(0) | N, \mathbf{p}_N \rangle \langle F, \mathbf{p}_F | a_{N'}^\dagger(\mathbf{p}_{N'}) a_N(\mathbf{p}_N) | I \rangle \\
&\times \sum_{M=p,n}^A \sum_{\sigma_{M'}} \int \frac{d^3\mathbf{p}_{M'}}{(2\pi)^3 \sqrt{2E_{M'}}} \frac{d^3\mathbf{p}_M}{(2\pi)^3 \sqrt{2E_M}} \delta_V^{(3)}(\mathbf{p}_M - \mathbf{p}_{M'} + \mathbf{q}) \\
&\times \langle M, \mathbf{p}_M | j^{\nu\dagger}(0) | M', \mathbf{p}_{M'} \rangle \langle I | a_M^\dagger(\mathbf{p}_M) a_{M'}(\mathbf{p}_{M'}) | F, \mathbf{p}_F \rangle.
\end{aligned} \tag{2.11}$$

Unfortunately, in general it is not known how to combine the one-body current matrix elements in the IA regime. One does not have any trivial connection between the one-particle states N, M and N', M' . Additional assumptions are needed in order to obtain a useful form of the hadronic tensor.

2.3 Plane wave IA

Within the *plane wave impulse approximation* (PWIA), one assumes that the one-particle state produced after the interaction is a plane wave and does not interact with the residual hadronic system. The final state can be factorized as follows:

$$|F, \mathbf{p}_F\rangle_A \rightarrow |X, \mathbf{p}_X\rangle \otimes |R, \mathbf{p}_R\rangle_{A-1}, \tag{2.12}$$

where X is a one-particle state, R is the residual hadronic system and $p_F = p_X + p_R$.

The inclusive cross section reads

$$d\sigma = \sum_{X,R} d\sigma_{X,R}. \tag{2.13}$$

As there are three distinguishable outgoing states, similar to (2.3), it can be expressed as

$$\frac{d\sigma}{d^3\mathbf{k}'} = \frac{1}{8(2\pi)^3} \frac{1}{E_k M_A E_{k'} E_X E_R} \frac{\alpha^2}{q^4} L_{\mu\nu} W^{\mu\nu}, \tag{2.14}$$

or

$$\frac{d\sigma}{d\Omega_{k'} dE_{k'}} = \frac{1}{8(2\pi)^3} \frac{E_{k'}}{E_k} \frac{1}{M_A E_X E_R} \frac{\alpha^2}{q^4} L_{\mu\nu} W^{\mu\nu}. \quad (2.15)$$

The summation over X, R and the integration over $d^3\mathbf{p}_X, d^3\mathbf{p}_R$ is already included in the hadronic tensor. Analogous to (2.11), one gets

$$\begin{aligned} W^{\mu\nu} &= \sum_{X,R,\sigma_I} \int d^3\mathbf{p}_X d^3\mathbf{p}_R \frac{(2\pi)^3}{V} \delta(E_F - M_A - \omega) \\ &\times \sum_{N=p,n}^A \sum_{\sigma_{N'}} \int \frac{d^3\mathbf{p}_{N'}}{(2\pi)^3 \sqrt{2E_{N'}}} \frac{d^3\mathbf{p}_N}{(2\pi)^3 \sqrt{2E_N}} \delta_V^{(3)}(\mathbf{p}_{N'} - \mathbf{p}_N - \mathbf{q}) \\ &\times \langle N', \mathbf{p}_{N'} | j^\mu(0) | N, \mathbf{p}_N \rangle \langle X, \mathbf{p}_X; R, \mathbf{p}_R | a_{N'}^\dagger(\mathbf{p}_{N'}) a_N(\mathbf{p}_N) | I \rangle \\ &\times \sum_{M=p,n}^A \sum_{\sigma_{M'}} \int \frac{d^3\mathbf{p}_{M'}}{(2\pi)^3 \sqrt{2E_{M'}}} \frac{d^3\mathbf{p}_M}{(2\pi)^3 \sqrt{2E_M}} \delta_V^{(3)}(\mathbf{p}_M - \mathbf{p}_{M'} + \mathbf{q}) \\ &\times \langle M, \mathbf{p}_M | j^{\nu\dagger}(0) | M', \mathbf{p}_{M'} \rangle \langle I | a_M^\dagger(\mathbf{p}_M) a_{M'}(\mathbf{p}_{M'}) | X, \mathbf{p}_X; R, \mathbf{p}_R \rangle. \end{aligned} \quad (2.16)$$

An additional assumption is that N', M' are the outgoing states and one-particle state X can be annihilated using $a_{N'}, a_{M'}$. Using (A.26), one obtains

$$\begin{aligned} W^{\mu\nu} &= \sum_{\sigma_X, R, \sigma_I} \int d^3\mathbf{p}_X d^3\mathbf{p}_R \frac{(2\pi)^3}{V} \delta(E_F - M_A - \omega) \\ &\times \sum_{N=p,n}^A \int \frac{d^3\mathbf{p}_N}{(2\pi)^3 \sqrt{2E_N}} \delta_V^{(3)}(\mathbf{p}_X - \mathbf{p}_N - \mathbf{q}) \\ &\times \langle X, \mathbf{p}_X | j^\mu(0) | N, \mathbf{p}_N \rangle \langle R, \mathbf{p}_R | a_N(\mathbf{p}_N) | I \rangle \Big|_{\tau_X = \tau_N} \\ &\times \sum_{M=p,n}^A \int \frac{d^3\mathbf{p}_M}{(2\pi)^3 \sqrt{2E_M}} \delta_V^{(3)}(\mathbf{p}_M - \mathbf{p}_X + \mathbf{q}) \\ &\times \langle M, \mathbf{p}_M | j^{\nu\dagger}(0) | X, \mathbf{p}_X \rangle \langle I | a_M^\dagger(\mathbf{p}_M) | R, \mathbf{p}_R \rangle \Big|_{\tau_X = \tau_M}. \end{aligned} \quad (2.17)$$

Note that this formula already implies the equality $\mathbf{p}_N = \mathbf{p}_M$.

2.3.1 Factorization

An essential point in the discussion is the factorization property. It allows one to express the electron-nucleus cross section as the elementary electron-nucleon cross section multiplied by the spectral function. The first key assumption, that the N', M' states are

the outgoing ones, has already been taken. Then, one needs to be able to combine the matrix elements of (2.17) into, e.g., $|\langle X, \mathbf{p}_X | j^\mu(0) | N, \mathbf{p} \rangle|^2$, $|\langle R, -\mathbf{p} | a_N(\mathbf{p}) | I \rangle|^2$. Therefore, in order to factorize the cross section in PWIA, one needs to equate the states N and M . Such a property was proven in, e.g., Ref. [30]. The proof discusses the conditions on which the matrix elements $\langle R, \mathbf{p}_R | a_N(\mathbf{p}_N) | I \rangle$ and $\langle I | a_M^\dagger(\mathbf{p}_M) | R, \mathbf{p}_R \rangle$ are non-vanishing. If the final state R is considered to be a plane wave, momentum conservation implies that $\mathbf{p}_{N,M} = -\mathbf{p}_R$. This condition allows to include the delta functions $\delta^{(3)}(\mathbf{p}_N + \mathbf{p}_R)$ and $\delta^{(3)}(\mathbf{p}_M + \mathbf{p}_R)$. Integrating over $d^3\mathbf{p}_N, d^3\mathbf{p}_M$ one obtains

$$\begin{aligned}
W^{\mu\nu} &= \sum_{\sigma_X, R, \sigma_I} \int d^3\mathbf{p}_X d^3\mathbf{p} \frac{(2\pi)^3}{V} \delta(E_F - M_A - \omega) \\
&\times \sum_{N=p,n}^A \frac{1}{(2\pi)^3 \sqrt{2E_N}} \delta_V^{(3)}(\mathbf{p}_X - \mathbf{p} - \mathbf{q}) \\
&\times \langle X, \mathbf{p}_X | j^\mu(0) | N, \mathbf{p} \rangle \langle R, -\mathbf{p} | a_N(\mathbf{p}) | I \rangle \\
&\times \sum_{M=p,n}^A \frac{1}{(2\pi)^3 \sqrt{2E_M}} \delta_V^{(3)}(\mathbf{p} - \mathbf{p}_X + \mathbf{q}) \\
&\times \langle M, \mathbf{p} | j^{\nu\dagger}(0) | X, \mathbf{p}_X \rangle \langle I | a_M^\dagger(\mathbf{p}) | R, -\mathbf{p} \rangle.
\end{aligned} \tag{2.18}$$

where $\mathbf{p}_N = \mathbf{p}_M = -\mathbf{p}_R \equiv -\mathbf{p}$.

The second argument is based on a sublime spin analysis in the basis of irreducible tensorial operators. As shown in Ref. [30], one can identify the spins σ_N, σ_M and take their average. In this calculation, it can be obtained by including an additional delta $\frac{1}{2}\delta_{N,M}$. One summation can be performed, and the hadronic tensor takes the form

$$\begin{aligned}
W^{\mu\nu} &= \frac{1}{2} \sum_{\sigma_X, R} \sum_{N=p,n}^A \int d^3\mathbf{p}_X d^3\mathbf{p} \delta(E_F - M_A - \omega) \delta^{(3)}(\mathbf{p}_X - \mathbf{p} - \mathbf{q}) \\
&\times \frac{1}{(2\pi)^6 2E_N} |\langle X, \mathbf{p}_X | j^\mu(0) | N, \mathbf{p} \rangle|^2 |\langle R, -\mathbf{p} | a_N(\mathbf{p}) | I \rangle|^2.
\end{aligned} \tag{2.19}$$

2.3.2 Spectral function

The spectral function allows one to write the hadronic tensor in more compact form. This function has an intuitive interpretation: it gives the probability of removing a nucleon of momentum \mathbf{p} from the target ground state leaving the residual system with excitation energy E . Such a nucleon is an off-shell particle. The expected form of the spectral

function is

$$P_N(\mathbf{p}, E) = \kappa \sum_R |\langle R, -\mathbf{p} | a_N(\mathbf{p}) | I \rangle|^2 \delta(E - M + M_A - E_R), \quad (2.20)$$

where κ is a normalization factor. The spectral function should be normalized as follows:

$$\begin{aligned} \int d^3\mathbf{p} dE P_p(\mathbf{p}, E) &= Z, \\ \int d^3\mathbf{p} dE P_p(\mathbf{p}, E) &= (A - Z). \end{aligned} \quad (2.21)$$

In order to find this formula within the hadronic tensor (2.19), one needs to perform few modifications. At first, the delta function needs to take the desired form. Recalling (2.12), one can see that in fact: $E_F = E_R + E_X$. Therefore, the delta function can be represented as

$$\begin{aligned} \delta(E_F - M_A - \omega) &= \delta(E_R + E_X - M_A - \omega) = \\ &= \int dE \delta(E - M + M_A - E_R) \delta(M - E - E_X + \omega), \end{aligned} \quad (2.22)$$

where M is the nucleon mass, which is constant. Using (A.26), one can find the normalization factor,

$$\kappa = \frac{1}{(2\pi)^6 2E_N}. \quad (2.23)$$

The hadronic tensor takes the form

$$\begin{aligned} W^{\mu\nu} &= \sum_{\sigma_X} \sum_{N=p,n}^A \int d^3\mathbf{p}_X d^3\mathbf{p} dE P_N(\mathbf{p}, E) \\ &\times |\langle X, \mathbf{p}_X | j^\mu(0) | N, \mathbf{p} \rangle|^2 \delta(M - E - E_X + \omega) \delta^{(3)}(\mathbf{p}_X - \mathbf{p} - \mathbf{q}), \end{aligned} \quad (2.24)$$

where

$$P_N(\mathbf{p}, E) = \frac{1}{(2\pi)^6 2E_N} \sum_R |\langle R, -\mathbf{p} | a_N(\mathbf{p}) | I \rangle|^2 \delta(E - M + M_A - E_R). \quad (2.25)$$

2.3.3 Factorized cross section

The elementary hadronic tensor $\omega_N^{\mu\nu}$ that corresponds to the lepton-nucleus scattering shall take a similar form as (1.16). As the state $\tau_X = \tau_N$, one can denote $N' \equiv X$ with

four-momentum $p' = (E_{p'}, \mathbf{p}')$. In (2.24), one can find the following equation:

$$\omega_N^{\mu\nu} \equiv \frac{1}{2} \sum_{\sigma_{N'}, \sigma_N} |\langle N', \mathbf{p}' | j^\mu(0) | N, \mathbf{p} \rangle|^2 \delta(M - E - E_{p'} + \omega) \delta^{(3)}(\mathbf{p}' - \mathbf{p} - \mathbf{q}). \quad (2.26)$$

Effective energy transfer, which accounts for the binding energy B , needs to be introduced:

$$\tilde{\omega} \equiv \omega - B. \quad (2.27)$$

The binding energy is the difference between the energy of the interacting nucleon, as if it was on the mass shell, and its energy in the nucleus; hence,

$$B = \sqrt{\mathbf{p}^2 + M^2} - (E_R - M_A). \quad (2.28)$$

On the other hand, the residual system excitation energy E can be expressed as the energy transfer ω minus the kinetic energy of the outgoing nucleon $T_{p'}$; thus,

$$E = \omega - T_{p'} = E_R - M_A + E_{p'} - T_{p'} = E_R - M_A + M, \quad (2.29)$$

and, therefore, $E_R - M_A = E - M$. Using that result, one can express the binding energy as

$$B = \sqrt{\mathbf{p}^2 + M^2} + E - M \quad (2.30)$$

and the effective energy transfer as

$$\tilde{\omega} = \omega + M - E - \sqrt{\mathbf{p}^2 + M^2}. \quad (2.31)$$

The effective four-momentum transfer reads $\tilde{q} \equiv (\tilde{\omega}, \mathbf{q})$. Therefore, one can take an elementary cross section in vacuum with four-momentum transfer \tilde{q} on the nucleon carrying momentum \mathbf{p} . The elementary hadronic tensor takes the form

$$\omega_N^{\mu\nu} = \frac{1}{2} \sum_{\sigma_{N'}, \sigma_N} |\langle N', \mathbf{p}' | j^\mu(0) | N, \mathbf{p} \rangle|^2 \delta^{(4)}(p' - p - \tilde{q}), \quad (2.32)$$

and the full hadronic tensor reads

$$W^{\mu\nu} = \sum_{N=p,n}^A \int d^3\mathbf{p}' d^3\mathbf{p} dE P_N(\mathbf{p}, E) \omega_N^{\mu\nu}, \quad (2.33)$$

where summation over N does not include spins anymore.

The nucleus has mass number A and atomic number Z , one can write

$$W^{\mu\nu} = \int d^3\mathbf{p}' d^3\mathbf{p} dE \left(Z P_p(\mathbf{p}, E) \omega_p^{\mu\nu} + (A - Z) P_n(\mathbf{p}, E) \omega_n^{\mu\nu} \right). \quad (2.34)$$

Finally, using (2.15) and integrating the delta $\delta^{(4)}(p' - p - \tilde{q})$ out, one obtains the differential cross section formula of the form

$$\left(\frac{d\sigma}{d\Omega_{k'}} \right)_A = \int d^3\mathbf{p} dE \chi \left(Z P_p(\mathbf{p}, E) \left(\frac{d\sigma_p}{d\Omega_{k'}} \right) + (A - Z) P_n(\mathbf{p}, E) \left(\frac{d\sigma_n}{d\Omega_{k'}} \right) \right), \quad (2.35)$$

where the kinematical factor reads

$$\chi = \frac{1}{2(2\pi)^3} \frac{M E_p}{M_A^2 E_R}, \quad (2.36)$$

and the elementary electron-nucleon cross section is of the form

$$\left(\frac{d\sigma_N}{d\Omega_{k'}} \right) = \frac{1}{4} \frac{E_{k'}^2}{E_k^2} \frac{1}{M E_p} \frac{\alpha^2}{q^4} L_{\mu\nu} \omega_N^{\mu\nu}, \quad (2.37)$$

where the elementary hadronic tensor $\omega_N^{\mu\nu}$ does not include $\delta^{(4)}(p' - p - \tilde{q})$ anymore.

Note that variables, such as E_p and E_R , are not measured in experiments. They can be expressed as

$$\begin{aligned} E_p &= E_R - M_A = E - M, \\ E_R &= E - M + M_A. \end{aligned} \quad (2.38)$$

2.3.4 Specific nucleon solution

Another approach has been presented by, e.g., J. A. Caballero et al. [33]. Suppose one knows how to obtain a solution for the specific nucleon on the given orbital in the target nucleus. Such a nucleon, with binding energy B , will be denoted as b with four-momentum $p_b = (E_b, \mathbf{p}_b)$. The following factorization of the initial hadronic state

can be performed:

$$|I\rangle \rightarrow \sum_b \int d^3\mathbf{p}_b (|R_b, -\mathbf{p}_b\rangle \otimes |b, \mathbf{p}_b\rangle) \alpha_b(\mathbf{p}_b), \quad (2.39)$$

where α_b is the function of momentum for the given orbital. The matrix element reads

$$\begin{aligned} \langle R, -\mathbf{p} | a_N(\mathbf{p}) | I \rangle &= \sum_b \int d^3\mathbf{p}_b \langle R, -\mathbf{p} | R_b, -\mathbf{p}_b \rangle \langle \emptyset | a_N(\mathbf{p}) | b, \mathbf{p}_b \rangle \alpha_b(\mathbf{p}_b) \\ &= \sum_b (2\pi)^3 \sqrt{2E_N} \delta_{R,R_b} \delta_{N,b} \int d^3\mathbf{p}_b \alpha_b(\mathbf{p}_b) \delta^{(3)}(\mathbf{p} - \mathbf{p}_b) \\ &= \sum_b (2\pi)^3 \sqrt{2E_N} \delta_{R,R_b} \delta_{N,b} \alpha_b(\mathbf{p}), \end{aligned} \quad (2.40)$$

and the spectral function as

$$\begin{aligned} \sum_{N=p,n}^A P_N(\mathbf{p}, E) &= \sum_{N=p,n}^A \frac{1}{(2\pi)^6 2E_N} \sum_R |\langle R, -\mathbf{p} | a_N(\mathbf{p}) | I \rangle|^2 \delta(E - M + M_A - E_R) \\ &= \sum_b \sum_{N=p,n}^A \sum_R \delta_{R,R_b} \delta_{N,b} \alpha_b^2(\mathbf{p}) \delta(E - M + M_A - E_R) \\ &= \sum_b \alpha_b^2(\mathbf{p}) \delta(E - M + M_A - E_R), \end{aligned} \quad (2.41)$$

where $\alpha_b^2(\mathbf{p})$ is the momentum distribution function.

The hadronic tensor takes the form

$$\begin{aligned} W^{\mu\nu} &= \sum_b \int d^3\mathbf{p}' d^3\mathbf{p} dE \alpha_b^2(\mathbf{p}) \delta(E - M + M_A - E_R) \\ &\quad \times \frac{1}{2} \sum_{\sigma_{N'}, \sigma_N} |\langle N', \mathbf{p}' | j^\mu(0) | N, \mathbf{p} \rangle|^2 \delta^{(4)}(p' - p - \tilde{q}). \end{aligned} \quad (2.42)$$

Using these results, one obtains the cross section formula

$$\begin{aligned}
\left(\frac{d\sigma_b}{d\Omega_{k'} dE_{k'} d\Omega_{p'}} \right)_A &= \sum_b \frac{dE_{p'}}{4(2\pi)^3} \frac{E_{k'} |\mathbf{p}'|}{E_k M_A E_R} \frac{\alpha^2}{q^4} \int d^3\mathbf{p} dE \alpha_b^2(\mathbf{p}) L_{\mu\nu} \omega^{\mu\nu} \\
&\times \delta(p' - p - \tilde{q}) \delta(E - M + M_A - E_R) \\
&= \sum_b \frac{dE_{p'}}{4(2\pi)^3} \frac{E_{k'} |\mathbf{p}'|}{E_k M_A E_R} \frac{\alpha^2}{q^4} \alpha_b^2(\mathbf{p}) L_{\mu\nu} \omega^{\mu\nu} \delta(E_{p'} + \sqrt{\mathbf{p}^2 + M^2} - \omega) \\
&= \sum_b \frac{1}{4(2\pi)^3} \frac{E_{k'} |\mathbf{p}'|}{E_k M_A E_R} \frac{\alpha^2}{q^4} \alpha_b^2(\mathbf{p}) L_{\mu\nu} \omega^{\mu\nu} \\
&= \sum_b \chi \left(\frac{d\sigma}{d\Omega_{k'}} \right) \alpha_b^2(\mathbf{p}),
\end{aligned} \tag{2.43}$$

where

$$\chi = \frac{1}{(2\pi)^3} \frac{E_k M E_p |\mathbf{p}'|}{E_{k'} M_A E_R}. \tag{2.44}$$

2.4 Relativistic PWIA

Within the *relativistic plane wave impulse approximation* (RPWIA), one obtains the initial nucleon state solving the Dirac equation with scalar and vector potentials. Therefore, the negative-energy solutions also need to be taken into consideration. The following analysis has been motivated by the work of J. A. Caballero et al. [33].

In QED, the hadronic current is of the form $\bar{\psi} \Gamma^\mu \psi$. Out of the four combinations of creation and annihilation operators, only the terms that produce particles in the final states are considered; hence,

$$\begin{aligned}
\bar{\psi}(x) \Gamma^\mu \psi(x) &= \int \frac{d^3\mathbf{p}}{\sqrt{2E_p} (2\pi)^3} \frac{d^3\mathbf{p}'}{\sqrt{2E_{p'}} (2\pi)^3} \sum_{s, s'} \\
&\times [a^\dagger(\mathbf{p}', s') \bar{u}(\mathbf{p}', s') \Gamma^\mu a(\mathbf{p}, s) u(\mathbf{p}, s) e^{-i(p' - p) \cdot x} \\
&+ a^\dagger(\mathbf{p}', s') \bar{u}(\mathbf{p}', s') \Gamma^\mu b^\dagger(\mathbf{p}, s) v(\mathbf{p}, s) e^{i(p' + p) \cdot x}].
\end{aligned} \tag{2.45}$$

One can see that the term $a^\dagger a$ has already been discussed, while the term $a^\dagger b^\dagger$ is new.

The final hadronic state factorization is the same as in the PWIA case (2.12). Therefore, the general cross section formula remains the same (2.15).

2.4.1 One-body current

The one-body current needs to be redefined to include new terms. One can see that the term $a^\dagger b^\dagger$ corresponds to the pair production process. Such process has the total symmetry sign (-1) , as compared to the scattering process. Therefore, by extending (2.7), the currents read

$$\begin{aligned} \mathcal{J}^\mu(\mathbf{x}) \approx & \sum_{N=p,n}^A \sum_{\sigma_{N'}} \int \frac{d^3 \mathbf{p}_{N'}}{(2\pi)^3 \sqrt{2E_{N'}}} \frac{d^3 \mathbf{p}_N}{(2\pi)^3 \sqrt{2E_N}} \Bigg|_{\tau_N=\tau_{N'}} \times \\ & \left(\langle N', \mathbf{p}'_N | j^\mu(\mathbf{x}) | N, \mathbf{p}_N \rangle a_{N'}^\dagger(\mathbf{p}_{N'}) a_N(\mathbf{p}_N) - \langle N', \mathbf{p}'_N; \bar{N}, \mathbf{p}_N | j^\mu(\mathbf{x}) | \emptyset \rangle a_{N'}^\dagger(\mathbf{p}_{N'}) b_N^\dagger(\mathbf{p}_N) \right), \end{aligned} \quad (2.46)$$

and

$$\begin{aligned} \mathcal{J}^{\nu\dagger}(\mathbf{x}) \approx & \sum_{M=p,n}^A \sum_{\sigma_{M'}} \int \frac{d^3 \mathbf{p}_{M'}}{(2\pi)^3 \sqrt{2E_{M'}}} \frac{d^3 \mathbf{p}_M}{(2\pi)^3 \sqrt{2E_M}} \Bigg|_{\tau_M=\tau_{M'}} \times \\ & \left(\langle M, \mathbf{p}_M | j^{\nu\dagger}(\mathbf{x}) | M', \mathbf{p}_{M'} \rangle a_M^\dagger(\mathbf{p}_M) a_{M'}(\mathbf{p}_{M'}) - \langle \emptyset | j^{\nu\dagger}(\mathbf{x}) | N', \mathbf{p}'_N; \bar{N}, \mathbf{p}_N \rangle b_M(\mathbf{p}_M) a_{M'}(\mathbf{p}_{M'}) \right), \end{aligned} \quad (2.47)$$

2.4.2 Hadronic tensor

As the one-body current changed, it also affects the hadronic tensor. The matrix elements in the current and the adjoint multiply; hence,

$$W^{\mu\nu} = \mathcal{W}^{\mu\nu} + \mathcal{Z}^{\mu\nu} + \mathcal{N}^{\mu\nu}, \quad (2.48)$$

where \mathcal{W} , \mathcal{Z} correspond to the contributions from the interacting nucleons of positive and negative respectively. \mathcal{N} denote the crossed term. This notation is consistent with [33].

The $\mathcal{W}^{\mu\nu}$ tensor is exactly the same as in the PWIA case; hence,

$$\begin{aligned} \mathcal{W}^{\mu\nu} = & \frac{1}{2} \sum_{\sigma_X, R} \sum_{N=p,n}^A \int d^3 \mathbf{p}_X d^3 \mathbf{p} \delta(E_F - M_A - \omega) \delta^{(3)}(\mathbf{p}_X - \mathbf{p} - \mathbf{q}) \\ & \times \frac{1}{(2\pi)^6 2E_N} |\langle X, \mathbf{p}_X | j^\mu(0) | N, \mathbf{p} \rangle|^2 |\langle R, -\mathbf{p} | a_N(\mathbf{p}) | I \rangle|^2. \end{aligned} \quad (2.49)$$

The $\mathcal{Z}^{\mu\nu}$ term take a similar form to (2.49). However, the arguments beyond (2.17) change. Because of the b^\dagger operator, the momentum relation is different: $\mathbf{p}_R = \mathbf{p}$, and, thus,

$$\begin{aligned} \mathcal{Z}^{\mu\nu} &= \frac{1}{2} \sum_{\sigma_X, R} \sum_{N=p, n}^A \int d^3\mathbf{p}_X d^3\mathbf{p} \delta(E_F - M_A - \omega) \delta^{(3)}(\mathbf{p}_X + \mathbf{p} - \mathbf{q}) \\ &\times \frac{1}{(2\pi)^6 2E_N} |\langle X, \mathbf{p}_X; \bar{N}, \mathbf{p} | j^\mu(0) | \emptyset \rangle|^2 \left| \langle R, \mathbf{p} | b_N^\dagger(\mathbf{p}) | I \rangle \right|^2. \end{aligned} \quad (2.50)$$

The crossed term reads

$$\begin{aligned} \mathcal{N}^{\mu\nu} &= -\frac{1}{2} \sum_{\sigma_X, R} \sum_{N=p, n}^A \frac{1}{(2\pi)^6 2E_N} \int d^3\mathbf{p}_X d^3\mathbf{p} \delta(E_F - M_A - \omega) \frac{(2\pi)^3}{V} \\ &\times \left[\delta_V^{(3)}(\mathbf{p}_X - \mathbf{p} - \mathbf{q}) \delta_V^{(3)}(\mathbf{p}_X + \mathbf{p} - \mathbf{q}) \right. \\ &\times \langle X, \mathbf{p}_X | j^\mu(0) | N, \mathbf{p} \rangle \langle \emptyset | j^{\nu\dagger}(0) | X, \mathbf{p}_X; \bar{N}, \mathbf{p} \rangle \langle R, -\mathbf{p} | a_N(\mathbf{p}) | I \rangle \langle I | b_N(\mathbf{p}) | R, \mathbf{p} \rangle \\ &+ \delta_V^{(3)}(\mathbf{p}_X + \mathbf{p} - \mathbf{q}) \delta_V^{(3)}(\mathbf{p}_X - \mathbf{p} - \mathbf{q}) \\ &\times \langle X, \mathbf{p}_X; \bar{N}, \mathbf{p} | j^\mu(0) | \emptyset \rangle \langle N, \mathbf{p} | j^{\nu\dagger}(0) | X, \mathbf{p}_X \rangle \langle R, \mathbf{p} | b_N^\dagger(\mathbf{p}) | I \rangle \langle I | a_N^\dagger(\mathbf{p}) | R, -\mathbf{p} \rangle \left. \right] \\ &= -\frac{1}{2} \sum_{\sigma_X, R} \sum_{N=p, n}^A \frac{1}{(2\pi)^6 2E_N} \int d^3\mathbf{p}_X d^3\mathbf{p} \delta(E_F - M_A - \omega) \\ &\times \left[\delta^{(3)}(\mathbf{p}_X - \mathbf{q}) \Big|_{\mathbf{p}=0} \right. \\ &\times \langle X, \mathbf{p}_X | j^\mu(0) | N, \mathbf{p} \rangle \langle \emptyset | j^{\nu\dagger}(0) | X, \mathbf{p}_X; \bar{N}, \mathbf{p} \rangle \langle R, -\mathbf{p} | a_N(\mathbf{p}) | I \rangle \langle I | b_N(\mathbf{p}) | R, \mathbf{p} \rangle \\ &+ \delta^{(3)}(\mathbf{p}_X - \mathbf{q}) \Big|_{\mathbf{p}=0} \\ &\times \langle X, \mathbf{p}_X; \bar{N}, \mathbf{p} | j^\mu(0) | \emptyset \rangle \langle N, \mathbf{p} | j^{\nu\dagger}(0) | X, \mathbf{p}_X \rangle \langle R, \mathbf{p} | b_N^\dagger(\mathbf{p}) | I \rangle \langle I | a_N^\dagger(\mathbf{p}) | R, -\mathbf{p} \rangle \left. \right]. \end{aligned} \quad (2.51)$$

2.4.3 Spectral functions

In order to keep the equations transparent, one should introduce the spectral functions.

Then, the positive and negative energy hadronic tensors read

$$\begin{aligned} \mathcal{W}^{\mu\nu} &= \frac{1}{2} \sum_{\sigma_X} \sum_{N=p, n}^A \int d^3\mathbf{p}_X d^3\mathbf{p} dE P_N(\mathbf{p}, E) |\langle X, \mathbf{p}_X | j^\mu(0) | N, \mathbf{p} \rangle|^2 \\ &\times \delta(M - E - E_X + \omega) \delta^{(3)}(\mathbf{p}_X - \mathbf{p} - \mathbf{q}), \end{aligned} \quad (2.52)$$

where

$$P_N(\mathbf{p}, E) = \frac{1}{(2\pi)^6 2E_N} \sum_R |\langle R, -\mathbf{p} | a_N(\mathbf{p}) | I \rangle|^2 \delta(E - M + E_I - E_R); \quad (2.53)$$

and

$$\begin{aligned} \mathcal{Z}_N^{\mu\nu} = & \frac{1}{2} \sum_{\sigma_X} \sum_{N=p,n}^A \int d^3\mathbf{p}_X d^3\mathbf{p} dE N_N(\mathbf{p}, E) |\langle X, \mathbf{p}_X; \bar{N}, \mathbf{p} | j^\mu(0) | \emptyset \rangle|^2 \\ & \times \delta(M - E - E_X + \omega) \delta^{(3)}(\mathbf{p}_X + \mathbf{p} - \mathbf{q}), \end{aligned} \quad (2.54)$$

where

$$N_N(\mathbf{p}, E) = \frac{1}{(2\pi)^6 2E_N} \sum_R |\langle R, \mathbf{p} | b_N^\dagger(\mathbf{p}) | I \rangle|^2 \delta(E - M + E_I - E_R). \quad (2.55)$$

However, the crossed term causes severe difficulties. It is not clear how to deal with the product of the matrix elements $\langle R, -\mathbf{p} | a_N(\mathbf{p}) | I \rangle$, $\langle I | b_N(\mathbf{p}) | R, \mathbf{p} \rangle$ and the adjoint.

2.4.4 Specific nucleon solution

The aforementioned difficulties can be overcome using the solution for a nucleon on the specific orbital in the nucleus. The procedure is similar to the PWIA case. However, antiparticles travel back in time, and, thus, they are a part of the residual, not the initial state. Similarly to (2.39), one takes

$$|R, \mathbf{p}\rangle \rightarrow \sum_b \int d^3\mathbf{p}_b (|I_b, \mathbf{p} - \mathbf{p}_b\rangle \otimes |\bar{b}, \mathbf{p}_b\rangle) \beta_b(\mathbf{p}_b). \quad (2.56)$$

The matrix element can be expressed as

$$\begin{aligned} \langle R, \mathbf{p} | b_N^\dagger(\mathbf{p}) | I \rangle &= \sum_b \int d^3\mathbf{p}_b \langle \bar{b}, \mathbf{p}_b | b_N^\dagger(\mathbf{p}) | \emptyset \rangle \langle I_b, \mathbf{p} - \mathbf{p}_b | I \rangle \beta_b(\mathbf{p}_b) \\ &= \sum_b (2\pi)^3 \sqrt{2E_N} \delta_{I, I_b} \delta_{N, b} \int d^3\mathbf{p}_b \beta_b(\mathbf{p}_b) \delta^{(3)}(\mathbf{p} - \mathbf{p}_b) \\ &= \sum_b (2\pi)^3 \sqrt{2E_N} \delta_{I, I_b} \delta_{N, b} \beta_b(\mathbf{p}), \end{aligned} \quad (2.57)$$

and the antiparticles spectral function as

$$\begin{aligned}
\sum_{N=p,n}^A N_N(\mathbf{p}, E) &= \sum_{N=p,n}^A \frac{1}{(2\pi)^6 2E_N} \sum_R \left| \langle R, \mathbf{p} | b_N^\dagger(\mathbf{p}) | I \rangle \right|^2 \delta(E - M + M_A - E_R) \\
&= \sum_b \sum_{N=p,n}^A \sum_R \delta_{I, I_b} \delta_{N, b} \beta_b^2(\mathbf{p}) \delta(E - M + M_A - E_R) \\
&= \sum_b \sum_R \delta_{R+N, R_b+b} \beta_b^2(\mathbf{p}) \delta(E - M + M_A - E_R) \\
&= \sum_b \beta_b^2(\mathbf{p}) \delta(E - M + M_A - E_R).
\end{aligned} \tag{2.58}$$

The functions α_b, β_b are real and the equations (2.40, 2.57) can be used to calculate the crossed term as

$$\begin{aligned}
\mathcal{N}^{\mu\nu} &= - \int d^3\mathbf{p}' d^3\mathbf{p} dE \alpha_b(\mathbf{0}) \beta_b(\mathbf{0}) \delta(E - M + M_A - E_R) \\
&\quad \times \frac{1}{2} \sum_{\sigma_{N'}, \sigma_N} \delta(M - E - E_{N'} + \omega) \delta^{(3)}(\mathbf{p}' - \mathbf{q}) \Big|_{\mathbf{p}=0} \\
&\quad \times \left[\langle N', \mathbf{p}' | j^\mu(0) | N, \mathbf{0} \rangle \langle \emptyset | j^{\nu\dagger}(0) | N', \mathbf{p}'; \bar{N}, \mathbf{0} \rangle \right. \\
&\quad \left. + \langle N', \mathbf{p}'; \bar{N}, \mathbf{0} | j^\mu(0) | \emptyset \rangle \langle N, \mathbf{0} | j^{\nu\dagger}(0) | N', \mathbf{p}' \rangle \right].
\end{aligned} \tag{2.59}$$

Here, the elementary hadronic tensors are given by

$$\omega^{\mu\nu} = \frac{1}{2} \sum_{\sigma_{N'}, \sigma_N} |\langle N', \mathbf{p}' | j^\mu(0) | N, \mathbf{p} \rangle|^2, \tag{2.60}$$

$$\zeta^{\mu\nu} = \frac{1}{2} \sum_{\sigma_{N'}, \sigma_N} |\langle X, \mathbf{p}_X; \bar{N}, \mathbf{p} | j^\mu(0) | \emptyset \rangle|^2, \tag{2.61}$$

$$\begin{aligned}
\eta^{\mu\nu} &= \frac{1}{2} \sum_{\sigma_{N'}, \sigma_N} \left[\langle N', \mathbf{p}' | j^\mu(0) | N, \mathbf{0} \rangle \langle \emptyset | j^{\nu\dagger}(0) | N', \mathbf{p}'; \bar{N}, \mathbf{0} \rangle \right. \\
&\quad \left. + \langle N', \mathbf{p}'; \bar{N}, \mathbf{0} | j^\mu(0) | \emptyset \rangle \langle N, \mathbf{0} | j^{\nu\dagger}(0) | N', \mathbf{p}' \rangle \right].
\end{aligned} \tag{2.62}$$

Finally, the cross section can be factorized as follows:

$$\begin{aligned}
\left(\frac{d\sigma_b}{d\Omega_{k'} dE_{k'} d\Omega_{p'}} \right)_A &= \frac{dE_{p'}}{4(2\pi)^3} \frac{E_{k'} |\mathbf{p}'|}{E_k M_A E_R} \frac{\alpha^2}{q^4} \int d^3 \mathbf{p} dE L_{\mu\nu} \\
&\times \left[\alpha_b^2(\mathbf{p}) \omega^{\mu\nu} \delta^{(3)}(\mathbf{p}' - \mathbf{p} - \mathbf{q}) + \beta_b^2(\mathbf{p}) \zeta^{\mu\nu} \delta^{(3)}(\mathbf{p}' + \mathbf{p} - \mathbf{q}) \right. \\
&+ \left. \alpha_b(\mathbf{0}) \beta_b(\mathbf{0}) \eta^{\mu\nu} \delta^{(3)}(\mathbf{p}' - \mathbf{q}) \Big|_{\mathbf{p}=\mathbf{0}} \right] \\
&\times \delta(M - E - E_{N'} + \omega) \delta(E - M + M_A - E_R) \\
&= \chi \left[\left(\frac{d\sigma_P}{d\Omega_{k'}} \right) \alpha_b^2(\mathbf{p}) + \left(\frac{d\sigma_N}{d\Omega_{k'}} \right) \beta_b^2(\mathbf{p}) + \left(\frac{d\sigma_C}{d\Omega_{k'}} \right) \alpha_b(\mathbf{0}) \beta_b(\mathbf{0}) \right],
\end{aligned} \tag{2.63}$$

where

$$\chi = \frac{1}{(2\pi)^3} \frac{E_k}{E_{k'}} \frac{M E_p |\mathbf{p}'|}{M_A E_R}. \tag{2.64}$$

One can see that the final equation reduces to (2.43) in the non-relativistic limit, i.e., $\beta_b(\mathbf{p}) = 0$.

2.5 Two-body interaction

Using the framework presented in this chapter, one can extend the calculations using the two-body current. Such a current takes the form

$$\begin{aligned}
\mathcal{J}_2^\mu(\mathbf{x}) &= \sum_{N=p,n}^A \sum_{M=p,n}^{A-1} \sum_{\sigma_{N'}, \sigma_{M'}} \int \frac{d^3 \mathbf{p}_{N'}}{(2\pi)^3 \sqrt{2E_{N'}}} \frac{d^3 \mathbf{p}_N}{(2\pi)^3 \sqrt{2E_N}} \int \frac{d^3 \mathbf{p}_{M'}}{(2\pi)^3 \sqrt{2E_{M'}}} \frac{d^3 \mathbf{p}_M}{(2\pi)^3 \sqrt{2E_M}} \\
&\times \langle N', \mathbf{p}_{N'}; M', \mathbf{p}_{M'} | j^\mu(\mathbf{x}) | N, \mathbf{p}_N; M, \mathbf{p}_M \rangle a_{N'}^\dagger(\mathbf{p}_{N'}) a_{M'}^\dagger(\mathbf{p}_{M'}) a_N(\mathbf{p}_N) a_M(\mathbf{p}_M).
\end{aligned} \tag{2.65}$$

In this order of approximation, the current is a sum of both one- and two-body contributions:

$$\mathcal{J}^\mu(\mathbf{x}) \approx \mathcal{J}_1^\mu(\mathbf{x}) + \mathcal{J}_2^\mu(\mathbf{x}). \tag{2.66}$$

Such an extension strongly affects the hadronic current; it now contains three separate parts:

$$W^{\mu\nu} = W_{11}^{\mu\nu} + W_{12}^{\mu\nu} + W_{22}^{\mu\nu}. \tag{2.67}$$

The $W_{11}^{\mu\nu}$ part, containing only the one-body current contributions, has already been calculated. The second term $W_{12}^{\mu\nu}$ contains both one- and two-body currents components (two different matrix elements). The last one $W_{22}^{\mu\nu}$ has only the two-body current contributions. The calculation of the two terms which include the two-body current contributions, cause severe difficulties.

Focusing only on the $W_{22}^{\mu\nu}$ tensor in the PWIA, one gets

$$\begin{aligned}
W_{22}^{\mu\nu} = & \sum_{\sigma_X, \sigma_Y, R, \sigma_I} \int d^3\mathbf{p}_X d^3\mathbf{p}_Y d^3\mathbf{p}_R \frac{(2\pi)^3}{V} \delta(E_F - M_A - \omega) \\
& \times \sum_{N=p,n}^A \sum_{M=p,n}^{A-1} \int \frac{d^3\mathbf{p}_N}{(2\pi)^3 \sqrt{2E_N}} \frac{d^3\mathbf{p}_M}{(2\pi)^3 \sqrt{2E_M}} \delta_V^{(3)}(\mathbf{p}_X + \mathbf{p}_Y - \mathbf{p}_N - \mathbf{p}_M - \mathbf{q}) \\
& \times \langle X, \mathbf{p}_X; Y, \mathbf{p}_Y | j^\mu(0) | N, \mathbf{p}_N; M, \mathbf{p}_M \rangle \langle R, \mathbf{p}_R | a_N(\mathbf{p}_N) a_M(\mathbf{p}_M) | I \rangle \\
& \times \sum_{O=p,n}^A \sum_{P=p,n}^{A-1} \int \frac{d^3\mathbf{p}_O}{(2\pi)^3 \sqrt{2E_O}} \frac{d^3\mathbf{p}_P}{(2\pi)^3 \sqrt{2E_P}} \delta_V^{(3)}(\mathbf{p}_O + \mathbf{p}_P - \mathbf{p}_X - \mathbf{p}_Y + \mathbf{q}) \\
& \times \langle O, \mathbf{p}_O; P, \mathbf{p}_P | j^{\nu\dagger}(0) | X, \mathbf{p}_X; Y, \mathbf{p}_Y \rangle \langle I | a_P^\dagger(\mathbf{p}_P) a_O^\dagger(\mathbf{p}_O) | R, \mathbf{p}_R \rangle.
\end{aligned} \tag{2.68}$$

As shown before, an essential feature allowing one to factorize such a cross section is the connection between P, N and M, O . Unfortunately, in this example such a property is not straightforward. Some authors, however, use the *factorization ansatz* to overcome this difficulty [34].

Chapter 3

Correlated nucleon pairs and the two-nucleon knockout

There are many mechanisms which contribute to lepton induced two-nucleon knockout events. The most natural seem to be the two-body current processes, also referred to as the meson exchange current (MEC) events. Here, the four-momentum is implicitly transferred to two nucleons that can be ejected to the continuum. The second class of contributions are the initial state correlations (ISC) that can lead to the 2p2h final states even in reactions mediated by the one-body currents. The third class of effects include all of the reactions that happen after the primary interaction. Often called the final state interactions (FSI), they blur the image of each event and lead to a variety of different final states. The aforementioned mechanisms are schematically presented in Fig. 3.1.

Good-quality data that can be used to study the role of ISC in the neutrino-nucleus scattering has been reported by the ArgoNeuT Collaboration [19]. Because of the technology used, an extraordinary reconstruction of outgoing proton tracks is available. A sample of events with exactly two protons and no pions reconstructed in the final state has been selected, however, there is not a lot of data and the statistical predictive power is low. In the data analysis, two interesting observables have been identified. The first one is an angle between the two outgoing protons in the laboratory frame of reference. ArgoNeuT found that the back-to-back configuration for such protons is favorable. For other events, a simple reconstruction procedure has been performed. Again, an excess in the number of events with the reconstructed initial back-to-back configuration has

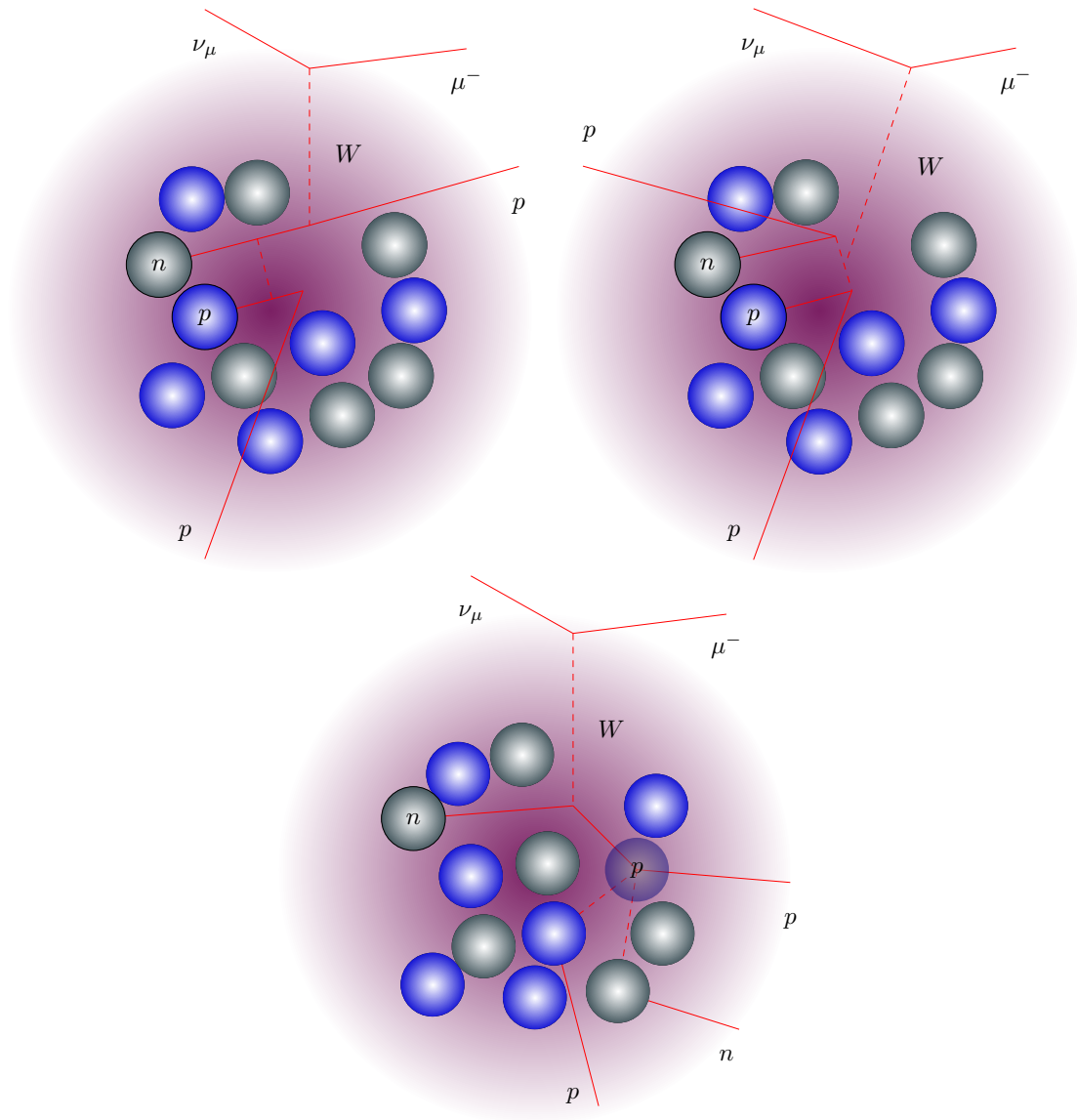


FIGURE 3.1: (Top left) nucleon-nucleon correlation and one-body interaction resulting in a two proton emission. (Top right) nucleon-nucleon correlation and two-body interaction resulting in a two proton emission. (Bottom) final state interactions that result in a similar multi-nucleon knockout.

been found. ArgoNeuT Collaboration argue that those configurations arise from the SRC nucleons.

Using Monte Carlo neutrino event generators, one can study the results of such experiments in order to identify promising observables in future experiments. For a review on MC neutrino event generators see, e.g., Ref. [26].

In this chapter, the ArgoNeuT Collaboration discoveries are confronted with the NuWro MC generator simulations results. The following discussion is an extended version of the author's works [21, 22]. The main arising question is whether NuWro contains physical

models that are sufficient to explain the ArgoNeuT results. A disagreement between the results would suggest that more sophisticated nuclear physics should be implemented in the neutrino MC simulation tools. Section 3.1 contains an introduction to the properties of the SRC nucleon pairs. Then, in Section 3.3 the ArgoNeuT experiment is briefly described. In Section 3.4, the NuWro MC neutrino event generator is characterized; the NuWro simulations configuration and the methods of data processing are presented. Sections 3.5 and 3.6 are devoted to the analysis of the selected observables. Finally, in Section 3.7, the results are discussed.

3.1 Short-range correlated nucleon pairs

Despite having a rather good understanding of the nature of the strong nucleon-nucleon interaction, the dynamics of atomic nuclei is not yet fully understood. General properties of such systems arise from nucleons keeping the Fermi-Dirac statistics. However, such Fermi systems are degenerate due to the nucleon short-range interactions in the *repulsive core* approximation.

There are many models that give satisfactory results in different applications. A class of models, useful in this study, use an *independent particle* (IP) approximation, where one can distinguish each nucleon in the system. The simplest model, that remains successful, in such a regime is the Fermi Gas of nucleons, where each one undergoes a mean-field potential of the square-well separately. The parametrization, including the Fermi momentum (k_F) and an average nucleon interaction energy, has been given in, e.g., [35]. Although widely exploited in many studies, the model has major limitations, especially in the two-body current reactions.

By solving the energy spectrum for a realistic nuclear potential, one obtains a more reliable result. The shape of such a potential changes from the Gaussian form for very light nuclei to the Wood-Saxon type for the heavier ones. This is a foundation of the Shell model of nuclear structure. The calculations for such model give extremely accurate distributions of the momentum and energy of nucleons. However, IP models struggle to predict the occupancy of the shells [36]. This effect is attributed to the short-range correlated (SRC) nucleon-nucleon pairs [37].

The SRC nucleon pairs have their mutual potential dominant over the mean field of the nucleus. They are responsible for the high-momentum tail (above k_F) of the nucleon momentum distribution [37]. Since the investigated nuclei are in the ground states, the total momentum of an SRC pair must be low. Therefore, nucleons in such pairs are in a characteristic back-to-back configuration. As presented in Ref. [36], no less than 20% of nucleons act in correlated pairs (for $A \geq 12$). Out of those, 90% take the form of high-momentum neutron-proton pairs. They can be interpreted as local fluctuations that act as deuteron nuclei within the nuclear system.

3.2 Theoretical approaches

The contributions of the SRC nucleon pairs in the 2p2h sector have been deeply investigated theoretically. The proper framework can be developed around the electron-induced reactions and then extended to the neutrino case. As mentioned before, it is not obvious if the cross section for the two-body current factorizes.

The formalism studied by *O. Benhar et al* [34, 38] uses the *factorization ansatz*. Neglecting the FSI, the authors point out two mechanisms resulting in electron-induced 2p2h final states. The first one arises from the one-body interaction with a new spectral function $P_{2h1p}(\mathbf{p}, E)$ that contains information about the ISC. Moreover, for the two-body interaction, one can introduce a two-nucleon spectral function $P(\mathbf{p}, \mathbf{p}', E)$. Such function in infinite nuclear matter has been calculated by *O. Benhar* and *A. Fabrocini* [39].

The factorization properties of the electroinduced two-nucleon knockout reaction has been investigated by *J. Ryckebusch et al* [40]. The factorized expression has been shown to be sensitive to the correlated nucleon pair center-of-mass momentum distribution. The first neutrino results within this formalism have also been presented [41]. Both of the aforementioned frameworks introduce short-range correlations using the symmetric correlation operator $\hat{\mathcal{G}}$ that modifies the wave function in the IP model. In terms of SRC, such operator is dominated by the central, tensor and spin-isospin components.

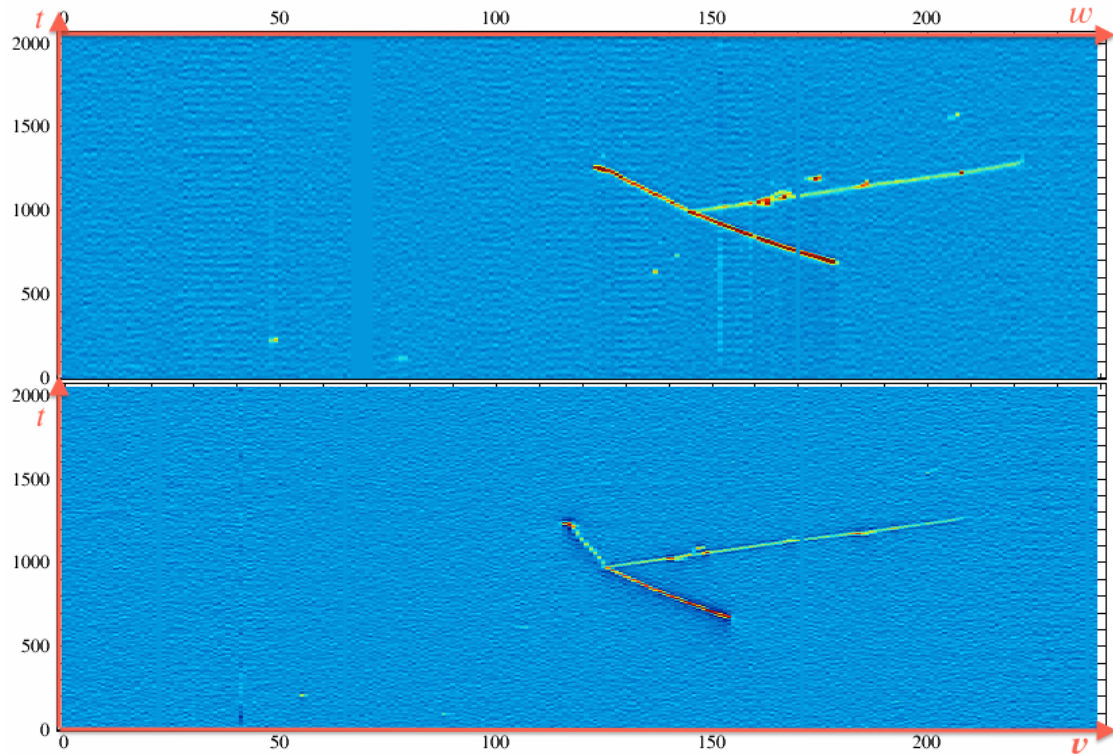


FIGURE 3.2: ArgoNeuT: two-dimensional views of one of the "hammer events," with a forward going muon and a back-to-back proton pair. Source: [19]. Transformations from the TPC wireplanes coordinates (w , t "collection plane" [top], v , t "induction plane" [bottom]) into lab coordinates are given in Ref. [42].

3.3 ArgoNeuT experiment

As presented in Refs [19, 42], the ArgoNeuT detector is a liquid argon TPC (LArTPC) with an active volume of $47 \times 40 \times 90 \text{ cm}^3$. The rectangular box is filled up with 240 kg (170 liters) of liquid argon and immersed in a 550 liter cryostat. The neutrino beam is led along the longest dimension of the chamber (the \hat{z} axis in the laboratory frame of reference). During the experiment the detector was set slightly off beam axis (TPC center located 26cm below the beam plane). For now, it is the only LArTPC to use a low energetic neutrino beam (0.1 – 10 GeV).

The source of neutrinos was the NuMI LE (low energy option) beam at the Fermi National Accelerator Laboratory (FNAL). ArgoNeuT operated during two runs of different NuMI horn configurations from September 2009 to February 2010. The total number of the detected CC neutrino events, after the efficiency correction, was 4488. 729 events were acquired in the ν -beam mode over the course of ~ 2 weeks. Other 3759 neutrino CC events were acquired in the $\bar{\nu}$ -beam mode with a large neutrino fraction over the

period of ~ 5 months. The average neutrino energy in the first beam was $\langle E_\nu \rangle \simeq 4$ GeV, while in the second beam it was $\langle E_\nu \rangle \simeq 10$ GeV.

In the experiment, the reconstruction of the outgoing particles is done only for the charged ones. Crossing the active volume they ionize free electron tracks. The uniform electric field, along the horizontal \hat{x} direction, makes the electrons drift to the two wire planes that collect the electron track image. The maximal drift length is 47 cm. The wire planes allow for the identification of signals from each of their 240 wires individually. They are rotated $\pm 60^\circ$ with respect to each other, and have their coordinates \hat{w} and \hat{v} . The time t after the signal detection is linear to the distance on the drift coordinate \hat{x} . Hence, the common wire planes coordinate is denoted as \hat{t} . In liquid argon there is no charge multiplication, and the signal pulse height is proportional to the amount of ionization charge. Summing over the charge of the entire track length gives precise calorimetric data and allows for a full three-dimensional reconstruction of the event. A sample wire planes view of the neutrino event is presented in Fig. 3.2.

As for the particles whose tracks are contained within the TPC, an energy loss is a known function of distance. This set-up is a powerful tool for particles identification. The technology used allows one to obtain a very low proton kinetic energy detection threshold of $T_p^{thr} = 21$ MeV, or 200 MeV/c of momentum, i.e., below the Fermi momentum of argon. For uncontained muons escaping in the forward direction, the momentum and charge identification was performed using the MINOS Near Detector (MINOS-ND) calorimeter located downstream from ArgoNeuT.

3.4 NuWro simulations

NuWro is a Monte Carlo event generator for the simulation of neutrino-nucleus scattering developed by the Wrocław Neutrino Group at the University of Wrocław over the past 10 years. It provides a complete description of (anti-)neutrino interactions on various nucleon or nucleus targets in the energy range from ~ 100 MeV to ~ 1 TeV. Currently, NuWro is being extended to also simulate the charged-lepton scattering processes [43].

There are three basic interaction channels on free nucleon targets:

- Charged-current quasielastic (CCQE) that includes also the elastic analog of (1) for neutral current reaction,
- Resonant single pion production (RES) covering a region of invariant hadronic mass $W \leq 1.6$ GeV; the dominant RES process is Δ resonance excitation

$$\nu_l + N \rightarrow l^- + \Delta \quad (3.1)$$

with N standing for either proton or neutron,

- Deep inelastic scattering (DIS): all of the inelastic processes with $W \geq 1.6$ GeV.

In the neutrino-nucleus interaction, an additional channel is considered:

- Meson-exchange current (MEC) – two-body current processes.

Neutrino-nucleus CCQE, RES, DIS and MEC reactions are modeled in the following steps:

- the primary interaction on one or two nucleons inside the nuclear target;
- the artificial model of final state interactions (FSI) affect all of the produced particles.

The NuWro FSI effects are described by custom made semiclassical intranuclear cascade (INC) model [23]. It includes pion absorption treated according to the model of *Oset et al* [44]. The mean free path is calculated based on a model with nuclear effects from Ref. [45]. In medium, nucleon-nucleon cross section is reduced relative to free nucleon scattering. The reduction is most important at low values of nucleon momentum and in regions with the highest density.

3.4.1 NuWro configurations

Being actively developed, NuWro provides many models and parametrizations that can be set during the configuration of the simulation. It offers a lot of flexibility for the composition of models used in an actual study. As described in Ref. [21], two different configurations have been used in the following analysis.

The first one is the default NuWro configuration:

- CCQE
 - local Fermi gas (LFG),
 - BBBA vector form factors,
 - dipole axial form factor with $M_A = 1.03$ MeV,
 - no coherent length effects for outgoing nucleon.
- RES
 - N- Δ axial form-factor in dipole parameterization with $M_A = 0.94$ GeV, $C_A^5(0) = 1.19$ [46],
 - nuclear target pion production reduced due to Δ in-medium self-energy implemented in the approximate way using results of [47],
 - non-resonant background added incoherently [48],
 - Δ finite life-time effects [23],
 - angular distribution of pions resulting from Δ decays modeled using results of ANL and BNL experimental measurements [49],
- DIS
 - PYTHIA fragmentation routines,
 - formation zone effects modeled as explained in [23],
- MEC
 - *Nieves et al* model with a momentum transfer cut $q \leq 1.2$ GeV/c,
 - in 95% of events interaction occurs on correlated back-to-back proton-neutron pairs,
 - finite state nucleons are assigned momenta using the phase space model [50],
 - no coherence length/formation zone effects for outgoing nucleons.

The difference in the second configuration arose in the CCQE channel, where the LFG model was replaced by the spectral function. The SF contained a contribution from the correlated nucleon-nucleon pairs. An important feature of the NuWro implementation of

the SF approach is the ability to distinguish whether an interaction occurs on a nucleon described by a mean-field approach or on a nucleon forming a correlated pair. In the latter, it is assumed that there is also a correlated nucleon that does not participate in the interaction, but, after initial interaction, propagates inside the nucleus. Its initial momentum is assumed to be opposite to the momentum of the interacting one.

Note that from the theorist perspective, it is not fully consistent to combine the MEC model of *Nieves et al* and the spectral function. However, both dynamical mechanisms provide events originating from a correlated nucleon pairs that can be distinguished on the level of data analysis.

The NuWro MC generator shares many common features with Monte Carlo generators NEUT and GENIE used by experimental groups [51]. Conclusions about NuWro performance with respect to the ArgoNeuT data are likely to also be applicable to other MC generators.

3.4.2 Normalization

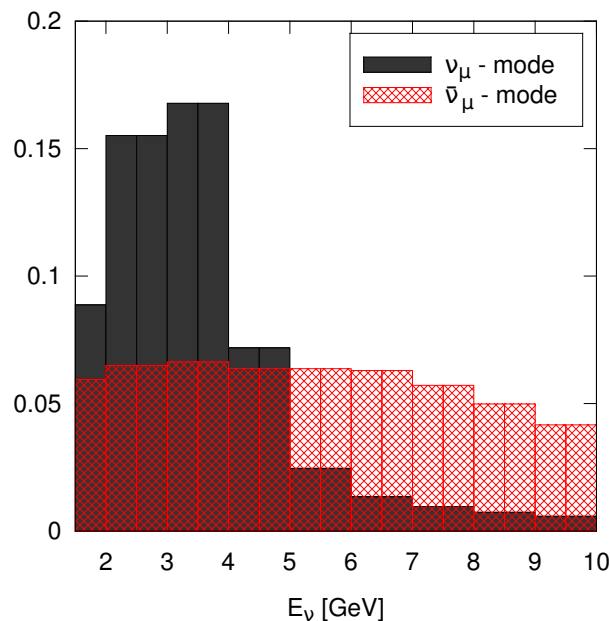


FIGURE 3.3: Shape of the two NuMI LE beams that were used in the NuWro simulations. The data is normalized to the same area.

In the analysis of ArgoNeuT Collaboration, neutrino events from both neutrino and antineutrino dominated runs were used. Proper normalization of the NuWro simulation

should be defined up to the total number of neutrino charged current events detected. The numbers of such events are 729 and 3759 in ν_μ and $\bar{\nu}_\mu$ modes respectively, so that the NuWro simulation was set to produce 2916000 and 15036000 neutrino CC events in two modes keeping their relative fractions fixed. The fluxes used in the simulations (see Fig. 3.3) were provided by the ArgoNeuT Collaboration.

3.4.3 Finite detector size

The active volume of the ArgoNeuT detector is limited and only the particles that have their tracks fully contained in the detector are identified. This eliminates a fraction of proton long track events. In order to simulate the detector finite-size effects, one can use the ArgoNeuT algorithm to calculate particle kinetic energy $T(R)$ (in the units of MeV) based on its track length R (in the units of cm) [52]:

$$T(R) = \frac{A}{b+1} R^{b+1}, \quad (3.2)$$

where the parameters for proton are $A = 17$ in the units of $\text{MeV}/\text{cm}^{(1+b)}$, and $b = -0.42$. For the reader's orientation, protons with a momentum of 500 MeV/c travel an average distance of 12.2 cm.

For each event, a position of occurrence within the TPC is uniformly drawn. Then using Eq. (3.2), one calculates the length of track for each proton. Attaching the length to the actual proton momentum directions, one can decide whether the track is fully contained in the TPC. Events with uncontained proton tracks are discarded.

3.4.4 Two proton events

	ν -mode (% of investigated 2p events)		$\bar{\nu}$ -mode (% of investigated 2p events)		% of 2p events in the total sample
ArgoNeuT	11	(37%)	19	(63%)	3.4%
NuWro: LFG	57979	(21.9%)	206955	(78.1%)	4.7%
NuWro: SF	61910	(22.1%)	217982	(77.9%)	4.9%

TABLE 3.1: Two-proton sample statistics from both ArgoNeuT and NuWro. The last column shows the efficiency corrected fraction of two-proton events without detector effects. The previous two columns show the contributions of two-proton events from both neutrino beams to the investigated subsample with detector effects.

ArgoNeuT performed a detail analysis of events with no pions and exactly two protons detected in the final state. Strictly speaking, the investigated data sample contains no charged pions with kinetic energy lower than 10 MeV, but according to NuWro the difference between two selections is negligible.

To follow the ArgoNeuT considerations, one can define NuWro samples of events in the same way. An arbitrary number of undetectable knocked out neutrons is allowed. ArgoNeuT collected 30 events of this type. The details about the analysis can be found in Tab. 3.1.

The 3.4% fraction of two-proton events in the ArgoNeuT data sample was estimated using the efficiency corrections [19]. Using NuWro, the distribution of muon angles for two-proton events has been checked. It is strongly peaked at $\sim 5^\circ$ without much difference for separated dynamical mechanisms. The contribution from muons with angles larger than 30° is very small, of the order of 3.5%. Therefore, any muon efficiency corrections were not introduced, because for angles lower than 30° ArgoNeuT muon detection efficiency is approximately constant and equal to $\sim 90\%$.

According to NuWro, the two-proton sample is strongly affected by the FSI effects. This is illustrated in Fig. 3.4, where fractions of two-proton (and no pion) events are shown as they result from various NuWro dynamical mechanisms. Without FSI two-proton events originate mainly from the MEC and also, in the second NuWro mode, from SRCs described by the SF. The FSI change this picture completely. With the FSI effects included there are many two-proton events coming from RES (pion absorption) and CCQE (nucleon rescattering). The small volume of the ArgoNeuT detector imposes an additional strong veto on large momentum protons. Almost all of the reconstructed protons have tracks shorter than ~ 30 cm corresponding to momentum of ~ 665 MeV/c (see also Fig. 1 in [19]). It is clear that good control over the FSI effects is a prerequisite for correct understanding of two-proton sample of events.

The NuWro predictions are in reasonable agreement with the ArgoNeuT results. Different relative contributions from ν and $\bar{\nu}$ modes can be attributed to statistical fluctuations.

In the next sections, the results are compared to the ArgoNeuT data for two-proton events that has not been efficiency corrected, and, in the NuWro results, only events

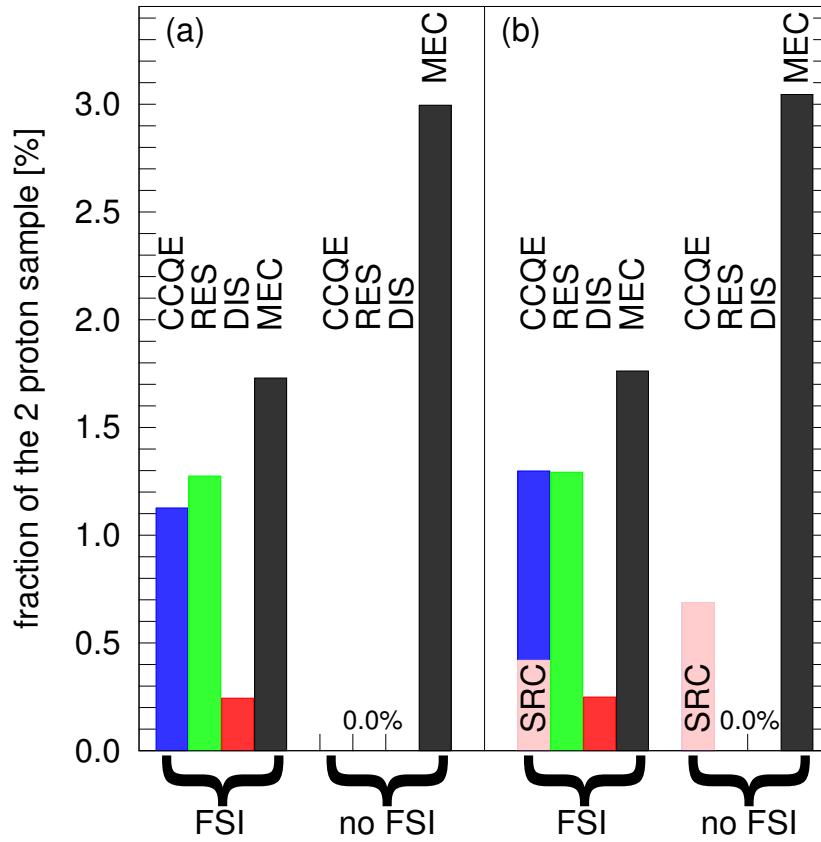


FIGURE 3.4: Impact of the FSI effects on the sample of two-proton events. Fractions of two-proton events with and without FSI effects are shown. Normalization is the same as in Tab. 3.1. (a) LFG model, (b) SF approach.

with the muon angle lower than 30° are considered.

3.5 Hammer events in the laboratory frame

The first interesting ArgoNeuT observable is a distribution of the cosine of the angle γ between two proton three-momenta in the laboratory frame. ArgoNeuT found an intriguing enhancement in the number of *hammer* events that are proton pairs in almost back-to-back configuration in the final state, defined as $\cos(\gamma) \leq -0.95$.

In NuWro, the distribution of $\cos \gamma$ in two-proton events were calculated, and compared with the experimental data in Fig. 3.5. The NuWro results were normalized to the same area.

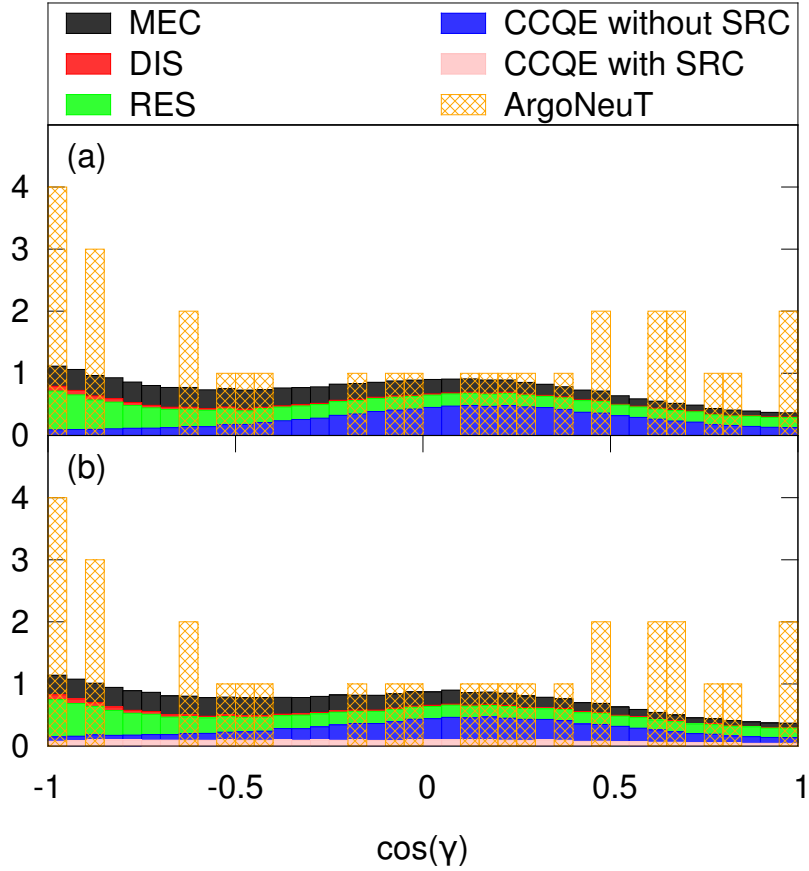


FIGURE 3.5: Distribution of the cosine of the angle between two protons in the final state. (a) LFG model, (b) SF approach.

The NuWro distributions are rather flat with two not very pronounced maxima: the first one at $\cos \gamma \sim -1$ and the second one at $\cos \gamma \sim 0$. According to NuWro, most of the hammer events come from the RES and MEC mechanisms.

Using the NuWro distributions one can calculate the probability of obtaining 4 or more events, $P(4+)$, in the first bin. Treating the NuWro results as the probability distribution and using the Poisson statistics, the following results were obtained:

- $P(4+) = 2.9\%$ for the LFG model;
- $P(4+) = 2.6\%$ for the SF approach.

The probabilities are similar and rather small in both cases. From the NuWro perspective, the appearance of at least four hammer events in a sample of 30 two-proton events is an interesting fact. The probability that it is merely a statistical fluctuation is only

about 3%. Certainly, better statistics data is required in order to draw a definite conclusion that MC event generators are unable to understand the appearance of so many hammer events.

ArgoNeuT proposed also to study a subsample of two-proton events by demanding that both protons have momenta larger than argon Fermi momentum. In this way, they received a reduced sample of only 19 events. In NuWro simulations, the similar requirement reduces the number of events by 30%; in very good agreement with 11/30 in the ArgoNeuT study.

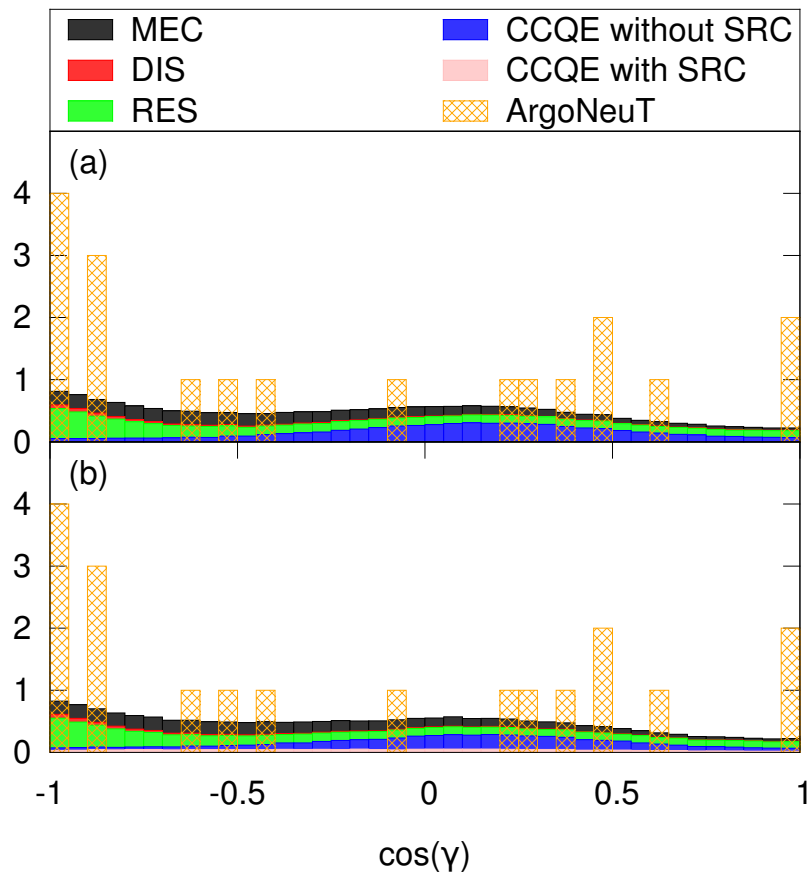


FIGURE 3.6: Distribution of the cosine of the angle between two protons in the final state. Subsample with both protons momenta above argon Fermi momentum. (a) LFG model, (b) SF approach.

In Fig. 3.6, the comparison of the experimental and NuWro results with the additional constraint on the proton momenta is presented. One can see that the shape of the NuWro distribution did not change significantly.

The probability of having four or more events, $P(4+)$, out of 19 in the first bin using NuWro results as the probability distribution read

- $P(4+) = 1.1\%$ for the LFG model;
- $P(4+) = 0.9\%$ for the SF approach.

Both probabilities are lower than before. Additionally, the detected hammer events were found to have both protons with similar momenta, i.e., $|\vec{p}_1| \simeq |\vec{p}_2| > k_F$ (by definition p_1 is more energetic than p_2 : $|\vec{p}_1| \geq |\vec{p}_2|$). Moreover, the events were characterized by typical values of missing transverse momentum $|p_{miss}^T| \geq 300$ MeV/c, where p_{miss}^T is defined as the length of the sum of three-momenta of all detectable particles (muon, protons) in the plane perpendicular to the beam direction. ArgoNeuT gives the explanation that laboratory frame hammer events originate mostly from the RES mechanism [53]. This agrees with the breakdown of the NuWro events in various interaction modes. The RES events contributing to the two-proton final states are those with pion being produced and subsequently absorbed inside the nucleus. While NuWro agrees with the ArgoNeuT on the dominant mechanism leading to hammer events, it cannot explain the fact that so many hammer events are contained in the samples of 30 or 19 ArgoNeuT events.

3.6 Reconstructed back-to-back nucleons before interaction

The ArgoNeuT Collaboration tried to identify a subsample of events occurring on correlated nucleon-nucleon pairs. ArgoNeuT proposed a procedure to reconstruct nucleon initial state configuration before the interaction assuming that it was a two nucleon state. The sample of 19 events discussed in Section 3.5 is further reduced by subtracting four (most likely RES) hammer events.

The incident neutrino energy and four-momentum transferred to the hadronic system are not known on the event-by-event basis. The precise reconstruction of their values is not possible because of the FSI effects blurring the image. ArgoNeuT attempted to approximate the nucleus recoil energy with the formula $T_{A-2} \approx \frac{(\vec{p}_{miss}^T)^2}{2M_{A-2}}$ (M_{A-2} is large enough and non-relativistic formula is a good approximation). The neutrino energy was reconstructed as

$$E_\nu = E_\mu + T_{p1} + T_{p2} + T_{A-2} + E_{miss}, \quad (3.3)$$

where T_{p1} and T_{p2} are proton kinetic energies, and $E_{miss} = 30$ MeV is the approximate energy needed to knock out a nucleon pair from an argon nucleus. With the reconstructed neutrino energy and information about the final state muon one can calculate three-momentum transfer. The final ansatz is that the three-momentum transfer was absorbed by the most energetic final state proton only, and both protons did not suffer from the FSI effects. In this way, one gets the initial state nucleon three-momenta and, in particular, the angle γ^i between both nucleons in the initial state. For events not occurring on nucleon-nucleon pairs the γ^i reconstruction procedure has no physical meaning.

ArgoNeuT found three reconstructed nucleon-nucleon pairs in approximately back-to-back configuration defined as $\cos\gamma^i \leq -0.9$. In the Fig. 6 in [19] three of them are shown in the bin $(-0.95, -0.9)$. ArgoNeuT also discussed the fourth event which lies on the bin boundary with $\cos\gamma^i \sim -0.89$. There are altogether six events in the region of $\cos\gamma^i \leq -0.8$.

Following the ArgoNeuT procedures, the NuWro sample of two-proton events was subtracted by

- hammer events in the LAB frame,
- events with less energetic proton momentum smaller than argon Fermi momentum.

For the remaining NuWro events the ArgoNeuT reconstruction procedure was performed.

In Fig. 3.7, the ArgoNeuT and NuWro distributions of $\cos\gamma^i$, normalized to the same area, are compared.

It is interesting to see that the NuWro distributions show a vast majority of events being reconstructed in the back-to-back initial state configuration. There are many reconstructed MEC events and also many SRC CCQE events in the NuWro SF mode. The appearance of many back-to-back SRC CCQE events in the SF mode is understandable, because in NuWro it is assumed that the three-momentum transfer is absorbed by one nucleon only. The excess of the MEC events may be surprising, because in NuWro the momentum transferred to the hadronic system is shared among both nucleons.

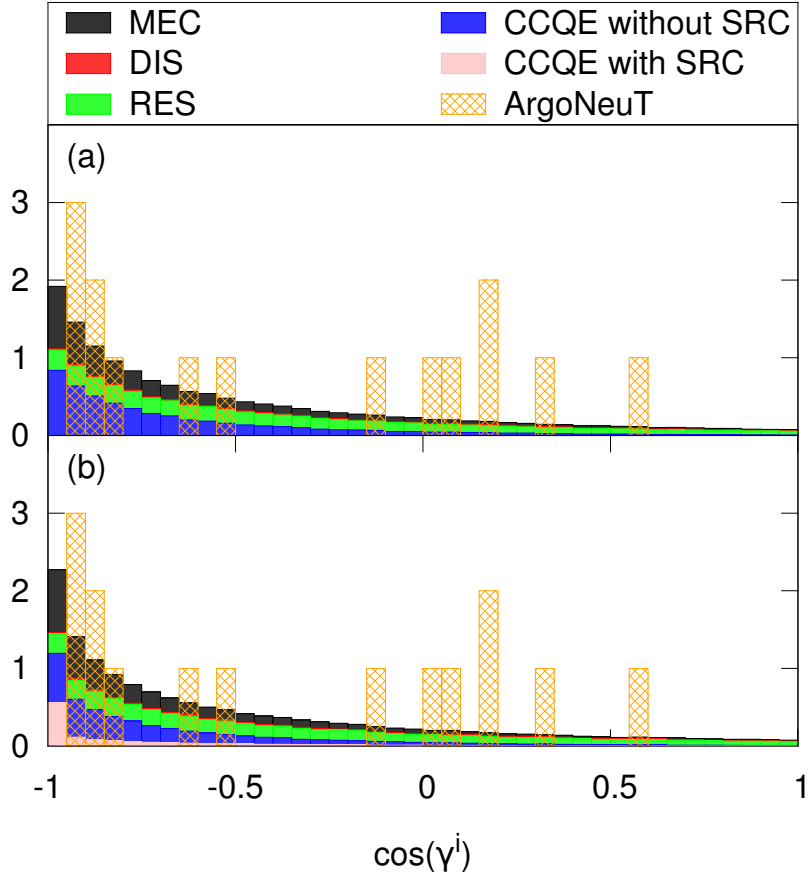


FIGURE 3.7: Distribution of the cosine of the reconstructed angle between two protons in the final state. (a) LFG model, (b) SF approach.

Using NuWro results as the probability distribution, the probabilities to have three (or more) events with $\cos \gamma^i \leq -0.9$ and six (or more) events with $\cos \gamma^i \leq -0.8$ were calculated. The results for the two NuWro modes are shown in Tab. 3.2.

	$\cos \gamma^i \leq -0.9$	$\cos \gamma^i \leq -0.8$
NuWro: LFG	$P(3+) = 65.0\%$	$P(6+) = 46.5\%$
NuWro: SF	$P(3+) = 70.9\%$	$P(6+) = 50.6\%$

TABLE 3.2: Probabilities of detecting three (or more) and six (or more) events with protons in the reconstructed initial back-to-back configuration according to NuWro.

The enhancements in the back-to-back configurations of reconstructed nucleons is fully understandable in terms of the NuWro simulations. The NuWro SF approach agrees with the data slightly better. Note that the reconstructed back-to-back sample of events contains also a significant contribution from the CCQE and RES events with no nucleon-nucleon initial state and the two-proton final state being the result of the FSI effects. This suggests that there may be a general physical argument explaining the shape of the $\cos \gamma^i$

distribution.

3.7 Discussion

So far, the strategy was always to follow closely the ArgoNeuT procedures. Two main ArgoNeuT results were studied. Having Monte Carlo generated events, one is able to discuss the interaction modes contributing to the experimentally selected samples of events [19]. In this way, it was confirmed that the hammer events in the LAB frame originate mostly from the RES events, and that a substantial fraction of the reconstructed back-to-back nucleon-nucleon pairs comes from the MEC mechanism and also from the CCQE mechanism on correlated nucleon-nucleon pairs.

In this section, the data/MC comparison will be more rigorous. As with the MC simulations, all the information relevant in the process can be used to investigate the origins of the selected phenomena.

3.7.1 Missing transverse momentum

The hammer events ($\cos(\gamma) \leq -0.95$) studied by the ArgoNeuT can be additionally characterized by the following conditions ¹:

- $|\vec{p}_1|, |\vec{p}_2| > k_F$,
- $|\vec{p}_{miss}^T| \geq 220 \text{ MeV}/c$,
- $\frac{|\vec{p}_1|}{|\vec{p}_2|} \leq 1.2$.

In the case of the ArgoNeuT two-proton sample, there are seven events (including four hammers) satisfying the above criteria ($7/30 \approx 23\%$). In the case of NuWro events, the subsample of only about 9% of two-proton events is accepted.

One of the additional conditions was defined in terms of missing transverse momentum. The accuracy of NuWro reproduction of the measured distribution of missing transverse momentum is investigated. Fig. 3.8 shows a distribution of p_{miss}^T from 29 ArgoNeuT two-proton events (one of the events exceeded the histogram range). The distribution

¹Private communication from Ornella Palamara

obtained with NuWro is shown also, and the NuWro results are normalized to the same histogram area. The enhancement of the events in the first bin (almost zero p_{miss}^T) in the SF NuWro configuration can be noticed. If both nucleons from the initial correlated nucleon pair did not suffer from FSI effects, the missing transverse momentum is exactly zero (in the NuWro SF mode nucleons in the initial correlated state have opposite three-momenta). In the simulation, the large missing transfer momentum events contain high momentum neutrons. Fig. 3.8 suggests that NuWro underestimates a probability of having such events.

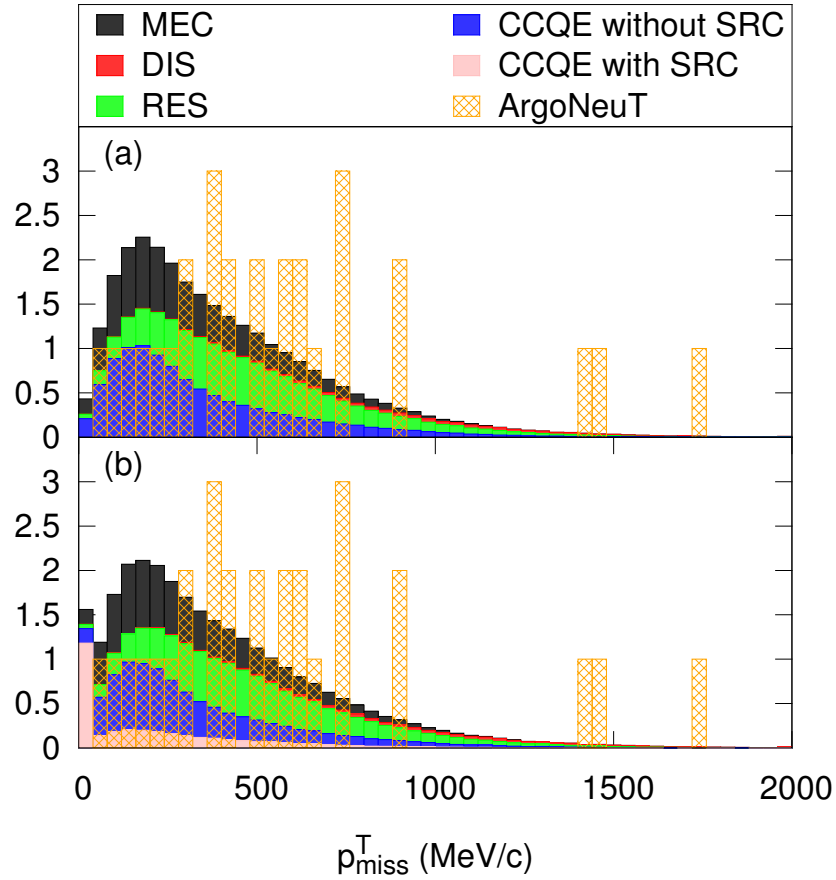


FIGURE 3.8: Missing transverse momentum distribution for 2 proton events. (a) LFG model, (b) SF approach.

The NuWro distribution of p_{miss}^T for the hammer events satisfying also $|\vec{p}_1|, |\vec{p}_2| > k_F$ and $\frac{|\vec{p}_1|}{|\vec{p}_2|} \leq 1.2$ has also been investigated. The distribution is shown in Fig 3.9. It is interesting to see that for $p_{miss}^T \geq 300$ MeV/c, the RES contribution starts to dominate. One should also expect many hammer events from the CCQE and MEC mechanisms characterized by $p_{miss}^T \sim 200$ MeV/c. They are, however, missing in the data. With better statistics, the experimental distribution of hammer events p_{miss}^T could provide useful information about the CCQE/MEC and RES mechanisms separately.

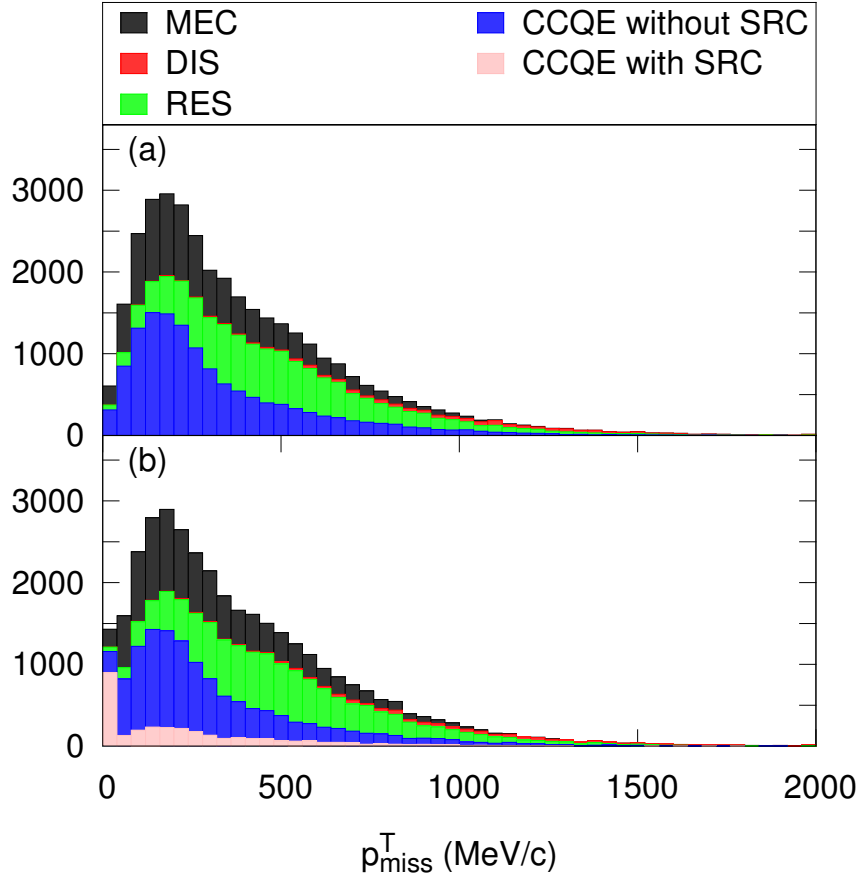


FIGURE 3.9: (Color online) Missing transverse momentum distribution for 2 proton hammer events. (a) LFG model, (b) SF approach.

3.7.2 Kinematics reconstruction procedure

An important analysis that is possible thanks to the information provided by NuWro is the reliability of the initial nucleon-nucleon reconstruction procedure, in the restricted subsample of 15 events.

Three quantities have been investigated. Namely, the incident neutrino energy, the value of three-momentum transfer, and the three-momentum transfer direction. The results are shown in Fig. 3.10 and in Tab. 3.3, where μ is the mean value, and σ is the standard deviation.

The reconstruction formula tends to underestimate the neutrino energy and, therefore, the value of the three-momentum transfer. This is due to the presence of undetected neutrons in the final state. In larger liquid argon detectors, such as MicroBooNE, the kinetic energy carried away by neutrons may be partially seen via interaction with visible

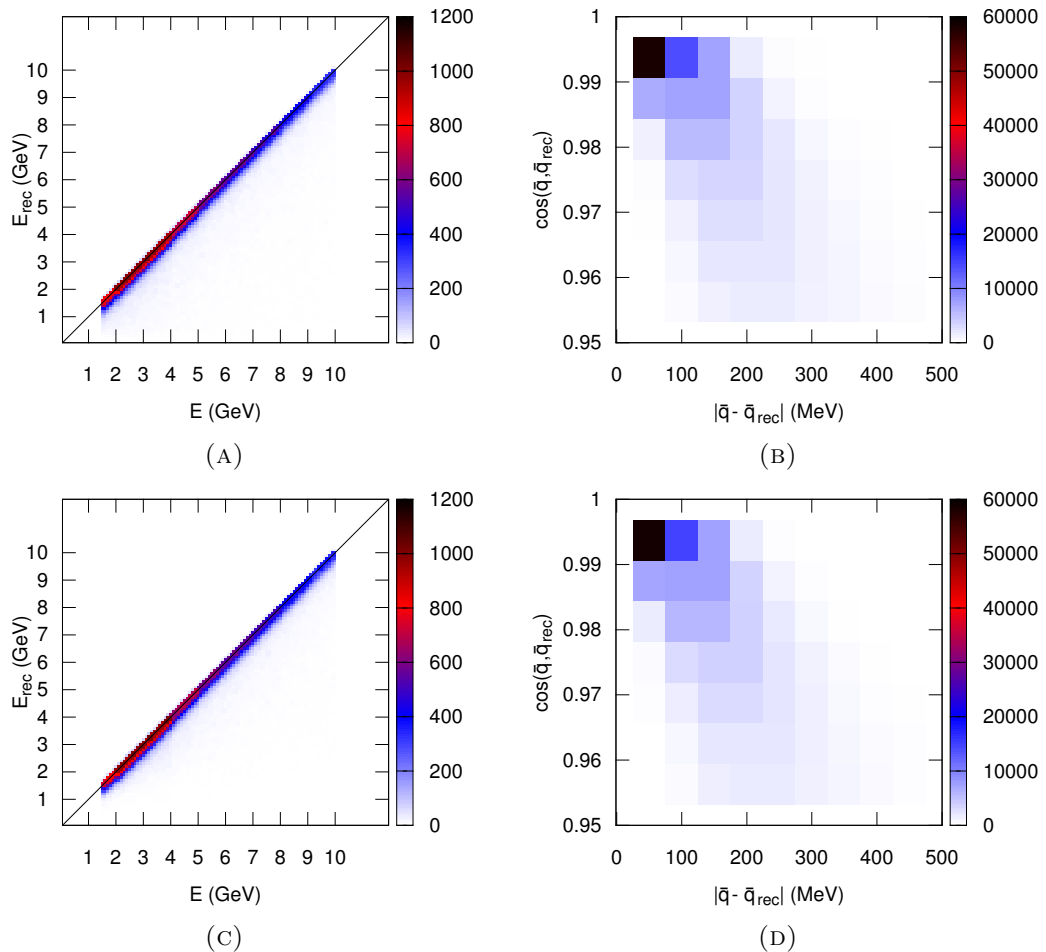


FIGURE 3.10: The reconstruction accuracy analysis using data from NuWro simulations: (A),(C) the reconstructed against the actual value of the incident neutrino energy for the LFG and SF approach respectively, (B),(D) cosine of the reconstructed and the real three-momentum transfer against the modulus of their difference for the LFG and SF approach respectively. Colors represent number of events in each bin.

	NuWro: LFG	NuWro: SF
$\mu(E'_\nu - E_\nu)$ [MeV]	-241	-238
$\sigma(E'_\nu - E_\nu)$ [MeV]	488	486
$\mu(1 - \cos(\vec{q}', \vec{q}))$	-0.04	-0.04
$\sigma(1 - \cos(\vec{q}', \vec{q}))$	0.079	0.079
$\mu(\vec{q}' - \vec{q})$ [MeV/c]	-244	-242
$\sigma(\vec{q}' - \vec{q})$ [MeV/c]	488	486

TABLE 3.3: The biases and standard deviations of reconstruction of neutrino energy, three-momentum transfer direction and three-momentum transfer value. From Eq. (3.3), it is clear that the quality of reconstruction of neutrino energy and momentum transfer are strongly correlated.

energy deposit making the reconstruction more precise. On the other hand, the direction of the three-momentum transfer is reconstructed quite accurately.

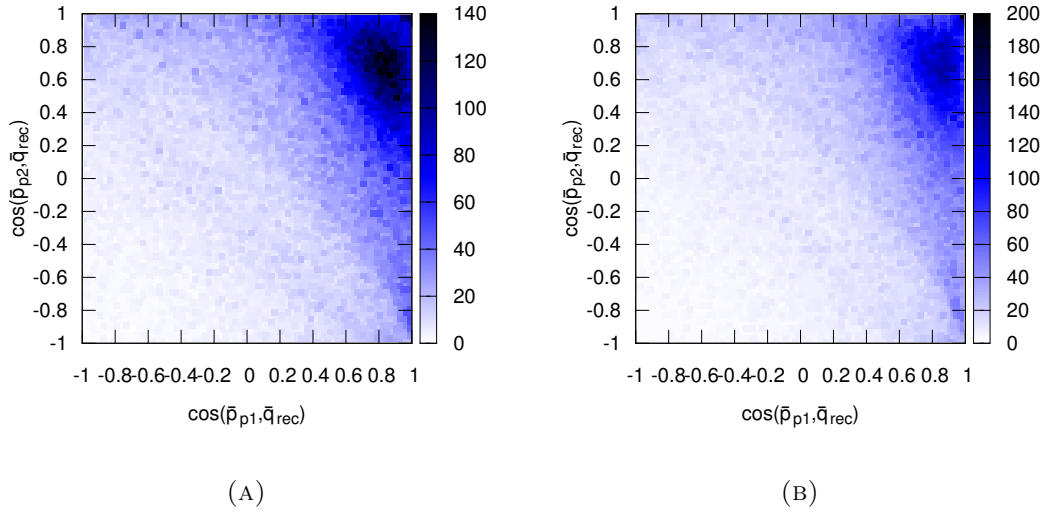


FIGURE 3.11: The cosine of the more energetic proton \vec{p}_{p1} and the reconstructed three-momentum transfer \vec{q}_{rec} versus the cosine of the less energetic proton \vec{p}_{p1} and the reconstructed three-momentum transfer \vec{q}_{rec} for: (A) the LFG model, (B) the SF approach. Colors represent number of events in each bin.

At this point, the problem of the shape of the $\cos \gamma^i$ distribution should be addressed. Momentum conservation implies that there is a correlation between \vec{q} , \vec{q}_{rec} and both nucleon three-momenta: \vec{p}_1 and \vec{p}_2 . As shown in Fig. 3.11, the distribution of $\cos(\vec{q}_{rec}, \vec{p}_1)$ peaks at ~ 0.85 . The distribution of $\cos(\vec{q}_{rec}, \vec{p}_2)$ is more diffused with a maximum at ~ 0.6 . The correlation between \vec{q}_{rec} and nucleon three-momenta is smeared out by the FSI effects and becomes weaker for events with a larger number of nucleon rescatterings inside a nucleus. Neglecting the contribution from the non-detected neutrons and nucleus recoil, one can expect that $\vec{q} \approx \vec{p}_1 + \vec{p}_2$ and $\vec{q} \approx \vec{q}_{rec}$. It is now clear that, if one defines $\vec{p}_1^i \equiv \vec{p}_1 - \vec{q}_{rec}$, as it is done in the ArgoNeuT paper, one should expect that \vec{p}_1^i and \vec{p}_2 will tend to be anti-parallel. Nuclear effects, such as the Fermi motion and, most importantly, the FSI, make the relation between \vec{p}_1^i and \vec{p}_2 more complicated. However, the basic feature of the distribution seen in Fig. 3.7, namely the peak in $\cos \gamma^i$ at -1, can be understood with presented above simple kinematical considerations. The shape seen in Fig. 3.7 is universal and does not depend much on the dynamical mechanism behind the appearance of the two-proton final state.

Conclusions

The aim of this thesis was to give an introduction to the theoretical and experimental approaches for studying the role of nucleon correlations in the lepton-nucleus interactions.

The theoretical foundation for the discussion is the standard result of the electron scattering off of the free nucleon. Then, the analysis is extended on the problem of complex hadronic targets. The electron-nucleus cross section is considered in various approximate regimes: IA, PWIA and RPWIA. The essential point of the analysis within the PWIA is the factorization property, i.e., expressing the cross section as an elementary electron-nucleon cross section multiplied by the weight-giving spectral function. The RPWIA is an extension to the PWIA case, where the bound target nucleon negative energy projections are also respected. A major limitation in extension of this framework to the two-body current case is emphasised. It is not straightforward whether the cross section for this reaction should factorize. Those calculations are the foundation for the development of the theoretical description of the lepton-induced two-nucleon knockout reactions.

The second part of this thesis was devoted to the ArgNeuT study of the two-proton and no pion events and its analysis using the simulations from the NuWro Monte Carlo event generator. The most spectacular ArgNeuT result is the appearance of several hammer-like events with almost back-to-back two-proton configuration in the LAB frame. According to NuWro, the probability of having that many hammer events varies from $\sim 3\%$ to $\sim 1\%$, depending on how the observable is defined. These results suggest that an important physical mechanism leading to two proton and no pion final states may be missing in NuWro and quite likely in other neutrino event generators as well.

Better statistical data from the awaited liquid argon MicroBooNE experiment will allow us to understand the situation better. Useful information about physical processes can be obtained from the missing transverse momentum distribution studies, allowing the examination of the nuclear physics models implemented in MCs. Another interesting observable is reconstructed angle between two nucleons in the hypothetical initial nucleon-nucleon state. ArgoNeuT reported an excess of back-to-back nucleons. This fact can be understood using models implemented in NuWro. This excess is argued to be kinematical in origin and is not directly related with existence of SRC nucleon pairs. Nevertheless, the details of the distribution shape is sensitive to SRC pairs, and it may be an important observable to investigate in future experiments.

Appendix A

Notation and conventions

In order to have consistent calculations and results a specific normalization has to be chosen. Here, the convention after *M. E. Peskin* and *D. V. Schroeder* [25] is used, together with the high-energy units: $\hbar = c = 1$.

A.1 Covariant notation

The following covariant notation is kept throughout this thesis. Moreover, whenever applicable, the Einstein summation convention is used.

The metric tensor reads

$$g_{\mu\nu} = g^{\mu\nu} = \begin{pmatrix} 1 & 0 & 0 & 0 \\ 0 & -1 & 0 & 0 \\ 0 & 0 & -1 & 0 \\ 0 & 0 & 0 & -1 \end{pmatrix}. \quad (\text{A.1})$$

The four-vectors are denoted as

$$x^\mu = (x^0, \mathbf{x}), \quad x_\mu = g_{\mu\nu}x^\nu = (x^0, -\mathbf{x}), \quad (\text{A.2})$$

where $x^0 \equiv t$ and $\mathbf{x} \equiv (x, y, z)$.

The scalar product is given by

$$x \cdot y \equiv x_\mu y^\mu = x^0 y^0 - \mathbf{x} \cdot \mathbf{y}. \quad (\text{A.3})$$

A.2 Dirac equation

The Dirac equation in the position representation reads

$$(i\gamma^\mu \partial_\mu - m)\psi(x) = 0, \quad (\text{A.4})$$

where $\psi(x)$ is a Dirac spinor.

Gamma matrices γ^μ are the generators of the Dirac algebra with the defining relation

$$\{\gamma^\mu, \gamma^\nu\} = 2g^{\mu\nu}. \quad (\text{A.5})$$

In this thesis, the following Dirac representation [54] is used

$$\gamma^0 = \begin{pmatrix} \mathbb{1} & 0 \\ 0 & -\mathbb{1} \end{pmatrix}, \quad \gamma^i = \begin{pmatrix} 0 & \sigma^i \\ -\sigma^i & 0 \end{pmatrix}, \quad (\text{A.6})$$

where σ^i are the Pauli matrices

$$\sigma^1 = \begin{pmatrix} 0 & 1 \\ 1 & 0 \end{pmatrix}, \quad \sigma^2 = \begin{pmatrix} 0 & -i \\ i & 0 \end{pmatrix}, \quad \sigma^3 = \begin{pmatrix} 1 & 0 \\ 0 & -1 \end{pmatrix}. \quad (\text{A.7})$$

The Hermitian conjugate of the gamma matrix is given by

$$(\gamma^\mu)^\dagger = \gamma^0 \gamma^\mu \gamma^0, \quad \gamma^0 \gamma^{\mu\dagger} \gamma^0 = \gamma^\mu. \quad (\text{A.8})$$

The commutator of gamma matrices gives

$$\sigma^{\mu\nu} \equiv \frac{i}{2} [\gamma^\mu, \gamma^\nu]. \quad (\text{A.9})$$

Commonly used notations are the Dirac adjoint and the Feynman slash notation: $\bar{\psi} \equiv \psi^\dagger \gamma^0$ and $\not{A} \equiv \gamma^\mu A_\mu$ respectively.

In the calculations, an important point are the traces of gamma matrices products:

$$\begin{aligned}
\text{Tr}(\mathbb{1}) &= 4, \\
\text{Tr}(\gamma^\mu) &= 0, \\
\text{Tr}(\gamma^\mu \gamma^\nu) &= 4 g^{\mu\nu}, \\
\text{Tr}(\gamma^\mu \gamma^\nu \gamma^\rho) &= 0, \\
\text{Tr}(\gamma^\mu \gamma^\nu \gamma^\rho \gamma^\sigma) &= 4 (g^{\mu\nu} g^{\rho\sigma} - g^{\mu\rho} g^{\nu\sigma} + g^{\mu\sigma} g^{\nu\rho}).
\end{aligned} \tag{A.10}$$

A.3 Normalization

In the Lorentz gauge $\partial_\mu A^\mu = 0$, the free photon field of four-momentum $p = (E_p, \mathbf{p})$ is given by

$$A_\mu(x) = \int \frac{d^3\mathbf{p}}{\sqrt{2E_p}(2\pi)^3} \sum_{r=1}^2 \left(c(\mathbf{p}, r) \epsilon_\mu(\mathbf{p}, r) e^{-ipx} + c^\dagger(\mathbf{p}, r) \epsilon_\mu^*(\mathbf{p}, r) e^{ipx} \right), \tag{A.11}$$

where ϵ_μ denotes the unit polarization vector with the polarization r . The operators c^\dagger, c are the bosonic creation and annihilation operators respectively, that satisfy the commutation relations

$$\begin{aligned}
[c(\mathbf{p}, s), c^\dagger(\mathbf{q}, r)] &= (2\pi)^3 \delta^{(3)}(\mathbf{p} - \mathbf{q}) \delta_{sr}, \\
[c(\mathbf{p}, s), c(\mathbf{q}, r)] &= 0, \\
[c^\dagger(\mathbf{p}, s), c^\dagger(\mathbf{q}, r)] &= 0.
\end{aligned} \tag{A.12}$$

The free Dirac spinor fields are given by

$$\begin{aligned}
\psi(x) &= \int \frac{d^3\mathbf{p}}{(2\pi)^3 \sqrt{2E_p}} \\
&\times \sum_s \left(a(\mathbf{p}, s) u(\mathbf{p}, s) e^{-ipx} + b^\dagger(\mathbf{p}, s) v(\mathbf{p}, s) e^{ipx} \right),
\end{aligned} \tag{A.13}$$

$$\begin{aligned}
\bar{\psi}(x) &= \int \frac{d^3\mathbf{p}}{(2\pi)^3 \sqrt{2E_p}} \\
&\times \sum_s \left(a^\dagger(\mathbf{p}, s) \bar{u}(\mathbf{p}, s) e^{ipx} + b(\mathbf{p}, s) \bar{v}(\mathbf{p}, s) e^{-ipx} \right),
\end{aligned} \tag{A.14}$$

where u, v denote the positive and negative energy free particle solutions of the Dirac equation respectively. The operators a^\dagger, a are the particle creation and annihilation operators, whereas, the operators b^\dagger, b are the antiparticle creation and annihilation operators. Those operators satisfy the anti-commutation relations

$$\begin{aligned} \{a(\mathbf{p}, s), a^\dagger(\mathbf{q}, r)\} &= \{b(\mathbf{p}, s), b^\dagger(\mathbf{q}, r)\} = (2\pi)^3 \delta^{(3)}(\mathbf{p} - \mathbf{q}) \delta_{sr}, \\ \{a(\mathbf{p}, s), a(\mathbf{q}, r)\} &= \{b(\mathbf{p}, s), b(\mathbf{q}, r)\} = 0, \\ \{a^\dagger(\mathbf{p}, s), a^\dagger(\mathbf{q}, r)\} &= \{b^\dagger(\mathbf{p}, s), b^\dagger(\mathbf{q}, r)\} = 0. \end{aligned} \quad (\text{A.15})$$

The Dirac spinor fields satisfy equal time anti-commutation relations

$$\begin{aligned} \{\psi(x), \psi^\dagger(y)\}|_{x_0=y_0} &= \delta^{(3)}(x - y), \\ \{\psi(x), \psi(y)\}|_{x_0=y_0} &= 0, \\ \{\psi^\dagger(x), \psi^\dagger(y)\}|_{x_0=y_0} &= 0. \end{aligned} \quad (\text{A.16})$$

The spinors u and v satisfy the Dirac equations in the momentum space

$$\begin{aligned} (\not{p} - m)u(\mathbf{p}, s) &= 0, \\ (\not{p} + m)v(\mathbf{p}, s) &= 0, \end{aligned} \quad (\text{A.17})$$

and are normalized as

$$u^\dagger(\mathbf{p}, s)u(\mathbf{p}, r) = 2E_{\mathbf{p}}\delta_{sr}, \quad \bar{u}(\mathbf{p}, s)u(\mathbf{p}, r) = 2m\delta_{sr}, \quad (\text{A.18})$$

$$v^\dagger(\mathbf{p}, s)v(\mathbf{p}, r) = 2E_{\mathbf{p}}\delta_{sr}, \quad \bar{v}(\mathbf{p}, s)v(\mathbf{p}, r) = -2m\delta_{sr}. \quad (\text{A.19})$$

One can choose

$$u(\mathbf{p}, s) = \sqrt{E_{\mathbf{p}} + m} \begin{pmatrix} \chi_s \\ \frac{\boldsymbol{\sigma} \cdot \mathbf{p}}{E_{\mathbf{p}} + m} \chi_s \end{pmatrix}, \quad (\text{A.20})$$

$$\chi_{s=\frac{1}{2}} = \begin{pmatrix} 1 \\ 0 \end{pmatrix}, \quad \chi_{s=-\frac{1}{2}} = \begin{pmatrix} 0 \\ 1 \end{pmatrix}, \quad (\text{A.21})$$

and

$$v(\mathbf{p}, s) = \sqrt{E_{\mathbf{p}} + m} \begin{pmatrix} -\frac{\boldsymbol{\sigma} \cdot \mathbf{p}}{E_{\mathbf{p}} + m} \xi_s \\ \xi_s \end{pmatrix}, \quad (\text{A.22})$$

$$\xi_{s=\frac{1}{2}} = \begin{pmatrix} 0 \\ 1 \end{pmatrix}, \quad \xi_{s=-\frac{1}{2}} = \begin{pmatrix} 1 \\ 0 \end{pmatrix}. \quad (\text{A.23})$$

The free particle states in the infinite volume are constructed to be invariant under Lorentz transformations, hence

$$|\mathbf{p}, s\rangle = \sqrt{2E_p} a^\dagger(\mathbf{p}, s) |\emptyset\rangle, \quad (\text{A.24})$$

and

$$\langle \mathbf{p}', s' | \mathbf{p}, s \rangle = (2\pi)^3 2E_p \delta^{(3)}(\mathbf{p} - \mathbf{p}') \delta_{s,s'}. \quad (\text{A.25})$$

Using (A.15,A.24), one can annihilate a one-particle state as

$$a(\mathbf{p}', s') |\mathbf{p}, s\rangle = (2\pi)^3 \sqrt{2E_p} \delta^{(3)}(\mathbf{p} - \mathbf{p}') \delta_{s,s'} |\emptyset\rangle, \quad (\text{A.26})$$

The fermion fields act on the one-particle states the following way

$$\begin{aligned} \psi(x) |\mathbf{k}, s\rangle &= u(\mathbf{k}, s) e^{-ik \cdot x} |\emptyset\rangle \\ \langle \mathbf{k}, s | \bar{\psi}(x) &= \langle \emptyset | \bar{u}(\mathbf{k}, s) e^{ik \cdot x}. \end{aligned} \quad (\text{A.27})$$

Appendix B

Cross section

B.1 Simple cross section definition

Let us suppose a particle passing through a layer of infinitesimal thickness δx , that has n scattering centers per unit volume. The probability that the particle undergoes an interaction is given by the formula

$$P_{int} = \sigma \cdot n \cdot \delta x, \quad (\text{B.1})$$

where σ is the coefficient of area dimension called the cross section.

The probability of transition through N such layers is given by the product of N elementary probabilities

$$P_{trans} = (1 - \sigma \cdot n \cdot \delta x)^N, \quad (\text{B.2})$$

and expressing $\delta x = \frac{x}{N}$, where x is the total depth, one obtains

$$P_{trans} = \left(1 - \sigma \cdot n \cdot \frac{x}{N}\right)^N. \quad (\text{B.3})$$

Taking the limit $N \rightarrow \infty$, the formula is of the form

$$P_{trans} = e^{-\sigma \cdot n \cdot x}, \quad (\text{B.4})$$

and taking the first-order approximation, one obtains

$$P_{trans} = 1 - \sigma \cdot n \cdot x, \quad P_{int} = \sigma \cdot n \cdot x. \quad (\text{B.5})$$

Dividing the probability of interaction by the time T of passing through the target, one obtains

$$\frac{P_{int}}{T} = \sigma \cdot n \cdot \frac{x}{T}. \quad (\text{B.6})$$

Then, $\frac{x}{T}$ can be identified as the relative velocity u_{rel} between the projectile and the target.

The general formula for the cross section reads

$$\sigma = \frac{P_{int}}{T \cdot \Phi}, \quad (\text{B.7})$$

where $\Phi = n \cdot u_{rel}$ is the flux of the scattering centers.

On the level of QFT, one usually assumes that $n = \frac{1}{V}$, where V is the volume of the system. The formula gets the form

$$\sigma = P_{int} \cdot \frac{V}{T \cdot u_{rel}}. \quad (\text{B.8})$$

Then, one calculates the probability of transition between the initial state Ψ_i in the time $t \rightarrow -\infty$ to the final state Ψ_f in the time $t \rightarrow \infty$. Such probability is given by

$$P_{int} \sim \left| \langle \Psi_f | \hat{S} | \Psi_i \rangle \right|^2, \quad (\text{B.9})$$

where \hat{S} is the scattering matrix containing information about the interaction.

B.2 Quantization in the finite volume

The following discussion is performed for the process of two interacting particles, as it is the most commonly considered situation. Here, the particles are denoted as: α with 4-momentum $p_\alpha = (E_\alpha, \mathbf{p}_\alpha)$ and β with 4-momentum $p_\beta = (E_\beta, \mathbf{p}_\beta)$. After the interaction, there are N_f particles produced with the four-momenta $p_i = (E_i, \mathbf{p}_i)$ for $i = 1, 2, \dots, N_f$.

The total initial (Ψ_i) and final (Ψ_f) states are of the form

$$\begin{aligned} |\Psi_i\rangle &= |\mathbf{p}_A\rangle \otimes |\mathbf{p}_B\rangle, \\ |\Psi_f\rangle &= \bigotimes_i^{N_f} |\mathbf{p}_i\rangle. \end{aligned} \quad (\text{B.10})$$

The probability of interaction is given by

$$dP = \left| \int_{box} \langle \Psi_f | \hat{S} | \Psi_i \rangle_{box} \right|^2 \cdot dN, \quad (\text{B.11})$$

where the density of states dN in the finite volume V is

$$dN = \prod_i^{N_f} \frac{V}{(2\pi)^3} d^3 \mathbf{p}_i. \quad (\text{B.12})$$

The relation between the states normalized in the box ($|\mathbf{p}\rangle_{box}$) and the state invariant under Lorentz measure ($|\mathbf{p}\rangle$) is given by

$$|\mathbf{p}\rangle_{box} = \frac{1}{\sqrt{2E_{\mathbf{p}}V}} |\mathbf{p}\rangle. \quad (\text{B.13})$$

Putting the results into (B.7), one obtains the general cross section formula

$$d\sigma = \frac{1}{2E_A 2E_B} \prod_{i=1}^{N_f} \left(\frac{d^3 \mathbf{p}_i}{2(2\pi)^3 E_{p_i}} \right) \frac{1}{\nu} \frac{1}{\Omega} \left| \langle \Psi_f | \hat{S} | \Psi_i \rangle \right|^2, \quad (\text{B.14})$$

where $\Omega = V \cdot T$ is the spacetime volume.

In order to square the S-matrix element, a square of the Dirac delta is needed. To perform such calculation, let us introduce a concept of Dirac delta in finite spacetime volume Ω .

At first, in the finite volume V , momenta can take only discrete values

$$\delta_V^{(3)}(\mathbf{p}_\alpha - \mathbf{p}_\beta) = \frac{1}{(2\pi)^3} \int_V d^3 \mathbf{x} e^{i\mathbf{x} \cdot (\mathbf{p}_\alpha - \mathbf{p}_\beta)} = \frac{V}{(2\pi)^3} \delta_{\mathbf{p}_\alpha, \mathbf{p}_\beta}. \quad (\text{B.15})$$

The delta function satisfies the property

$$\lim_{V \rightarrow \infty} \delta_V^{(3)}(\mathbf{p}_\alpha - \mathbf{p}_\beta) = \delta^{(3)}(\mathbf{p}_\alpha - \mathbf{p}_\beta). \quad (\text{B.16})$$

Note, that it is an artificial concept that enhance the transparency of calculations and whenever used it should be interpreted as

$$\int_V d^3\mathbf{p}_\alpha \delta_V^{(3)}(\mathbf{p}_\alpha - \mathbf{p}_\beta) \rightarrow \sum_{\mathbf{p}_\alpha} \delta_{\mathbf{p}_\alpha, \mathbf{p}_\beta}. \quad (\text{B.17})$$

As opposed to the infinite volume Dirac delta, the Kronecker delta can be squared. This can be used in the following way

$$\begin{aligned} \left(\delta_V^{(3)}(\mathbf{p}_\alpha - \mathbf{p}_\beta)\right)^2 &= \delta_V^{(3)}(\mathbf{p}_\alpha - \mathbf{p}_\beta) \cdot \delta_V^{(3)}(\mathbf{p}_\alpha - \mathbf{p}_\beta) = \frac{V}{(2\pi)^3} \delta_{\mathbf{p}_\alpha, \mathbf{p}_\beta} \cdot \frac{V}{(2\pi)^3} \delta_{\mathbf{p}_\alpha, \mathbf{p}_\beta} \\ &= \frac{V}{(2\pi)^3} \delta_V^{(3)}(\mathbf{p}_\alpha - \mathbf{p}_\beta). \end{aligned} \quad (\text{B.18})$$

Similarly, if one assumes that the process is cyclic in time with a period T obtains

$$(\delta_T(E_\alpha - E_\beta))^2 = \frac{T}{2\pi} \delta_T(E_\alpha - E_\beta), \quad (\text{B.19})$$

and finally, for the spacetime volume Ω

$$\left(\delta_\Omega^{(4)}(p_\alpha - p_\beta)\right)^2 = \frac{\Omega}{(2\pi)^4} \delta_\Omega^{(4)}(p_\alpha - p_\beta). \quad (\text{B.20})$$

B.3 Feynman rules in QED

The following set of Feynman rules [24] has been used to construct the $i\hat{S}$ matrix (with the four-momentum transfer q):

- Multiply by a factor $(-i)$ for each order of the perturbation expansion.
- Each of the vertices contributes with a factor of $(-ie \mathcal{J}_\mu(x) e^{-iq \cdot x})$ integrated over d^4x , where
 - the leptonic current reads: $j_\mu(x) = \bar{\psi}(x) \gamma_\mu \psi(x)$,
 - the hadronic current reads: $\mathcal{J}_\mu(x) = \bar{\psi}(x) \Gamma_\mu \psi(x)$
- Virtual photon propagator reads $\frac{-i}{(2\pi)^4} \frac{g^{\mu\nu}}{q^2}$.
- Integrate the four-momentum transfer (q) in every internal line.

Appendix C

Electron-nucleon scattering

C.1 Dirac delta integration

The electron-nucleon sixfold differential cross section formula (1.14) with the Dirac delta function released out of the hadronic tensor (1.16) can be rewritten as

$$\frac{d\sigma}{d^3\mathbf{k}'d^3\mathbf{p}'} = \frac{1}{4} \frac{1}{E_k E_p E_{k'} E_{p'}} \frac{\alpha^2}{q^4} L_{\mu\nu} W^{\mu\nu} \delta^{(4)}(p' - p - k + k'). \quad (\text{C.1})$$

Next, one can use the fact that $d^3\mathbf{k}' = |\mathbf{k}'|^2 d|\mathbf{k}'| d\Omega_{k'} = |\mathbf{k}'| E_{k'} dE_{k'} d\Omega_{k'}$ with negligible electron mass ($|\mathbf{k}'| = E_{k'}$) and obtain

$$\frac{d\sigma}{d\Omega_{k'}} = dE_{k'} d^3\mathbf{p}' \frac{1}{4} \frac{E_{k'}}{E_k} \frac{1}{E_p E_{p'}} \frac{\alpha^2}{q^4} L_{\mu\nu} W^{\mu\nu} \delta^{(4)}(p' - p - q). \quad (\text{C.2})$$

Four differentiation dimensions can be reduced using the Dirac delta. At first, one can integrate over $d^3\mathbf{p}'$ and obtain

$$\frac{d\sigma}{d\Omega_{k'}} = dE_{k'} \frac{1}{4} \frac{E_{k'}}{E_k} \frac{1}{E_p E_{p'}} \frac{\alpha^2}{q^4} L_{\mu\nu} W^{\mu\nu} \delta(E_{p'} - E_p - \omega) \Big|_{\mathbf{p}'=\mathbf{q}=\mathbf{k}-\mathbf{k}'}. \quad (\text{C.3})$$

However, because of the constraints one cannot simply put $\omega = E_k - E_{k'}$, because of the constraints and the fact that $E_{k'}$ and $E_{p'}$ are correlated. In order to manipulate the

delta function, one needs to recall a property

$$\delta(f(x)) = \sum_{x_0} \frac{\delta(x - x_0)}{\left| \frac{df}{dx}(x_0) \right|}, \quad (\text{C.4})$$

where x_0 are the roots of the $f(x)$ function. Now it can shown that

$$\delta(E_{p'}^2 - (E_p + \omega)^2) = \frac{1}{2E_{p'}} \delta(E_{p'} - (E_p + \omega)) \quad (\text{C.5})$$

remembering that all of the variables are non-negative and the function $f(E_{p'}) = E_{p'}^2 - (E_p + \omega)^2$ has only one root: $E_{p'0} = E_p + \omega$. One continues with

$$\begin{aligned} \frac{1}{2E_{p'}} \delta(E_{p'} - (E_p + \omega)) &= \delta(E_{p'}^2 - (E_p + \omega)^2) = \delta(E_{p'}^2 - E_p^2 - 2E_p\omega - \omega^2) \\ &= \delta(\mathbf{q}^2 - \omega^2 - 2E_p\omega) = \delta(-q^2 - 2E_p\omega) \\ &= \delta(q^2 + 2E_p\omega) = \frac{1}{2E_p} \delta\left(\omega + \frac{q^2}{2E_p}\right) \Bigg|_{\omega_0 = -\frac{q^2}{2E_p}} \\ &= \frac{1}{2E_p} \delta\left(E_k - E_{k'} - 2\frac{E_k E_{k'}}{E_p} \sin^2 \frac{\theta}{2}\right), \end{aligned} \quad (\text{C.6})$$

where the fact that $q^2 = -4E_k E_{k'} \sin^2 \frac{\theta}{2}$ has been used. The cross section formula is now in the form

$$\frac{d\sigma}{d\Omega_{k'}} = dE_{k'} \frac{1}{4} \frac{E_{k'}}{E_k} \frac{1}{E_p^2} \frac{\alpha^2}{q^4} L_{\mu\nu} W^{\mu\nu} \delta\left(E_k - E_{k'} - 2\frac{E_k E_{k'}}{E_p} \sin^2 \frac{\theta}{2}\right). \quad (\text{C.7})$$

Now, one can finally focus on the $E_{k'}$ variable. Using the same strategy, one obtains

$$\delta\left(E_k - E_{k'} - 2\frac{E_k E_{k'}}{E_p} \sin^2 \frac{\theta}{2}\right) = \frac{1}{1 + 2\frac{E_k}{E_p} \sin^2 \frac{\theta}{2}} \delta\left(E_{k'} - 2\frac{E_k}{1 + \frac{E_k}{E_p} \sin^2 \frac{\theta}{2}}\right), \quad (\text{C.8})$$

and therefore

$$\frac{d\sigma}{d\Omega_{k'}} = dE_{k'} \frac{1}{4} \frac{E_{k'}}{E_k} \frac{1}{E_p^2} \frac{\alpha^2}{q^4} L_{\mu\nu} W^{\mu\nu} \frac{1}{1 + 2\frac{E_k}{E_p} \sin^2 \frac{\theta}{2}} \delta\left(E_{k'} - \frac{E_k}{1 + 2\frac{E_k}{E_p} \sin^2 \frac{\theta}{2}}\right). \quad (\text{C.9})$$

Finally, integrating over $dE_{k'}$, one gets

$$\frac{d\sigma}{d\Omega_{k'}} = \frac{1}{4} \frac{E_{k'}^2}{E_k^2} \frac{1}{E_p^2} \frac{\alpha^2}{q^4} L_{\mu\nu} W^{\mu\nu}. \quad (\text{C.10})$$

C.2 Leptonic tensor calculation

The leptonic tensor is given by

$$\begin{aligned}
L_{\mu\nu} &= \frac{1}{2} \sum_{s,s'} (\bar{u}(\mathbf{k}', s') \gamma_\mu u(\mathbf{k}, s)) (\bar{u}(\mathbf{k}', s') \gamma_\nu u(\mathbf{k}, s))^* \\
&= \frac{1}{2} \sum_{s,s'} \bar{u}(\mathbf{k}', s') \gamma_\mu u(\mathbf{k}, s) \bar{u}(\mathbf{k}, s) \gamma_0 \gamma_\nu^\dagger \gamma_0 u(\mathbf{k}', s') \\
&= \frac{1}{2} \sum_{s,s'} \bar{u}(\mathbf{k}', s') \gamma_\mu u(\mathbf{k}, s) \bar{u}(\mathbf{k}, s) \gamma_\nu u(\mathbf{k}', s')
\end{aligned} \tag{C.11}$$

According to the normalization convention (A.18), the projection on the positive energy wave functions reads

$$\sum_s u(\mathbf{k}, s) \bar{u}(\mathbf{k}, s) = \not{k} + m. \tag{C.12}$$

Then, one obtains

$$\begin{aligned}
L_{\mu\nu} &= \frac{1}{2} \sum_{s,s'} \bar{u}^\alpha(\mathbf{k}', s') \gamma_\mu^{\alpha\beta} u^\beta(\mathbf{k}, s) \bar{u}^\rho(\mathbf{k}, s) \gamma_\nu^{\rho\sigma} u^\sigma(\mathbf{k}', s') \\
&= \frac{1}{2} \sum_{s,s'} u^\sigma(\mathbf{k}', s') \bar{u}^\alpha(\mathbf{k}', s') \gamma_\mu^{\alpha\beta} u^\beta(\mathbf{k}, s) \bar{u}^\rho(\mathbf{k}, s) \gamma_\nu^{\rho\sigma} \\
&= \frac{1}{2} (\not{k}' + m)^{\sigma\alpha} \gamma_\mu^{\alpha\beta} (\not{k} + m)^{\beta\rho} \gamma_\nu^{\rho\sigma} \\
&= \frac{1}{2} \text{Tr}[(\not{k}' + m) \gamma_\mu (\not{k} + m) \gamma_\nu].
\end{aligned} \tag{C.13}$$

Using (A.10) and setting electron mass $m \simeq 0$, one obtains

$$L_{\mu\nu} = 2(k'_\mu k_\nu + k'_\nu k_\mu - g_{\mu\nu} k' \cdot k). \tag{C.14}$$

C.3 Hadronic tensor calculation

The hadronic tensor is given by

$$\begin{aligned}
H^{\mu\nu} &= \frac{1}{2} \sum_{s,s'} \bar{u}(\mathbf{p}', s') \Gamma^\mu u(\mathbf{p}, s) (\bar{u}(\mathbf{p}', s') \Gamma^\nu u(\mathbf{p}, s))^* \\
&= \frac{1}{2} \sum_{s,s'} \bar{u}(\mathbf{p}', s') \Gamma^\mu u(\mathbf{p}, s) \bar{u}(\mathbf{p}, s) \gamma^0 \Gamma^{\nu\dagger} \gamma^0 u(\mathbf{p}', s').
\end{aligned} \tag{C.15}$$

Similarly to the leptonic tensor calculation, using (C.12), one gets

$$H^{\mu\nu} = \frac{1}{2} \text{Tr} \left[(\not{p}' + M) \Gamma^\mu (\not{p} + M) (\gamma^0 \Gamma^{\nu\dagger} \gamma^0) \right]. \quad (\text{C.16})$$

In order to have fewer gamma matrices in the calculation, one can use the other form of the effective interaction vertex (hadronic current), which is equivalent for on-shell particles. One can use

$$i\sigma^{\mu\nu} = g^{\mu\nu} - \gamma^\mu \gamma^\nu = \gamma^\nu \gamma^\mu - g^{\mu\nu}, \quad (\text{C.17})$$

and obtain

$$\begin{aligned} i\sigma^{\mu\nu} q_\nu &= i\sigma^{\mu\nu} (p' - p)_\nu \\ &= [(\gamma^\nu \gamma^\mu - g^{\mu\nu}) p'_\nu - (g^{\mu\nu} - \gamma^\mu \gamma^\nu) p_\nu] \\ &= [(\gamma \cdot p') \gamma^\mu - (p' + p)^\mu + \gamma^\mu (\gamma \cdot p)]. \end{aligned} \quad (\text{C.18})$$

Then, using the Dirac equation and its conjugate, one gets

$$\bar{u}(\mathbf{p}', s') i\sigma^{\mu\nu} q_\nu u(p, s) = \bar{u}(\mathbf{p}', s') [2M\gamma^\mu - (p' + p)^\mu] u(p, s), \quad (\text{C.19})$$

that is known as the *Gordon decomposition identity*:

$$\bar{u}(\mathbf{p}', s') \gamma^\mu u(p, s) = \bar{u}(\mathbf{p}', s') \left[\frac{(p' + p)^\mu}{2M} + \frac{i\sigma^{\mu\nu} (p' - p)_\nu}{2M} \right] u(p, s). \quad (\text{C.20})$$

The equation (C.19) can be used to obtain

$$\Gamma^\mu(q^2) = \left(F_1(q^2) + F_2(q^2) \right) \gamma^\mu - F_2(q^2) \frac{(p' + p)^\mu}{2M}. \quad (\text{C.21})$$

For the Hermitian adjoint holds

$$\gamma^0 \Gamma^{\mu\dagger} \gamma^0 = \gamma^0 \left((F_1 + F_2) \gamma^{\mu\dagger} - F_2(q^2) \frac{(p' + p)^{\mu\dagger}}{2M} \right) \gamma^0 = \Gamma^\mu. \quad (\text{C.22})$$

With the new form of the Γ^μ vertex, the hadronic tensor can be expressed as

$$\begin{aligned}
H^{\mu\nu} &= \frac{1}{2} \text{Tr} \left[(\not{p}' + M) \Gamma^\mu (\not{p} + M) (\gamma^0 \Gamma^{\nu\dagger} \gamma^0) \right] \\
&= \frac{1}{2} \text{Tr} \left[(\not{p}' + M) \left((F_1 + F_2) \gamma^\mu - F_2 \frac{(p' + p)^\mu}{2M} \right) (\not{p} + M) \left((F_1 + F_2) \gamma^\nu - F_2 \frac{(p' + p)^\nu}{2M} \right) \right] \\
&= \frac{1}{2} (F_1 + F_2)^2 \text{Tr} [(\not{p} + M) \gamma^\mu (\not{p} + M) \gamma^\nu] \\
&\quad - \frac{1}{2} (F_1 + F_2) \frac{F_2}{2M} (p' + p)^\mu \text{Tr} [(\not{p} + M) (\not{p} + M) \gamma^\nu] \\
&\quad - \frac{1}{2} (F_1 + F_2) \frac{F_2}{2M} \text{Tr} [(\not{p} + M) \gamma^\mu (\not{p} + M)] (p' + p)^\nu \\
&\quad + \frac{1}{2} \frac{F_2^2}{4M^2} (p' + p)^\mu (p' + p)^\nu \text{Tr} [(\not{p} + M) \gamma^\mu (\not{p} + M) \gamma^\nu].
\end{aligned} \tag{C.23}$$

Using (A.10), the traces can be resolved in the following way

$$\begin{aligned}
H^{\mu\nu} &= 2(F_1 + F_2)^2 (p'^\mu p^\nu + p'^\nu p^\mu - g^{\mu\nu} p' \cdot p + g^{\mu\nu} M^2) \\
&\quad - (F_1 + F_2) F_2 (p' + p)^\mu (p' + p)^\nu + 2 \frac{F_2^2}{4M^2} (p' + p)^\mu (p' + p)^\nu (p' \cdot p + M^2).
\end{aligned} \tag{C.24}$$

It is convenient to keep the result in two terms: proportional to $(F_1 + F_2)^2$ and to $(F_1^2 - \frac{F_2^2}{4M^2} q^2)$. The term proportional to $(F_1 + F_2) F_2$ can be turned into $(F_1 + F_2)^2$, leaving the term $(F_1^2 - F_2^2)$. Therefore, one has

$$\begin{aligned}
H^{\mu\nu} &= 2(F_1 + F_2)^2 (p'^\mu p^\nu + p'^\nu p^\mu + g^{\mu\nu} (M^2 - p' \cdot p) - \frac{1}{2} (p' + p)^\mu (p' + p)^\nu) \\
&\quad + (F_1^2 - F_2^2) (p' + p)^\mu (p' + p)^\nu + 2 \frac{F_2^2}{4M^2} (p' + p)^\mu (p' + p)^\nu (p' \cdot p + M^2) \\
&= 2(F_1 + F_2)^2 (p'^\mu p^\nu + p'^\nu p^\mu + g^{\mu\nu} (M^2 - p' \cdot p) - \frac{1}{2} (p' + p)^\mu (p' + p)^\nu) \\
&\quad + 2(p' + p)^\mu (p' + p)^\nu \left(\frac{F_2^2}{4M^2} (p' \cdot p - M^2) + \frac{1}{2} F_1^2 \right).
\end{aligned} \tag{C.25}$$

The last step is to get rid of the p' variable. One obtains

$$\begin{aligned}
H^{\mu\nu} &= 2(F_1 + F_2)^2(p'^{\mu}p^{\nu} + p'^{\nu}p^{\mu} + g^{\mu\nu}\frac{q^2}{2} - \frac{1}{2}(p' + p)^{\mu}(p' + p)^{\nu}) \\
&\quad + 2\left(\frac{1}{2}F_1^2 - \frac{F_2^2}{4M^2}\frac{q^2}{2}\right)(p' + p)^{\mu}(p' + p)^{\nu} \\
&= (F_1 + F_2)^2(g^{\mu\nu}q^2 - (p' - p)^{\mu}(p' - p)^{\nu}) + \left(F_1^2 - \frac{q^2}{4M^2}F_2^2\right)(p' + p)^{\mu}(p' + p)^{\nu} \\
&= (F_1 + F_2)^2(g^{\mu\nu}q^2 - q^{\mu}q^{\nu}) + \left(F_1^2 - \frac{q^2}{4M^2}F_2^2\right)(q + 2p)^{\mu}(q + 2p)^{\nu} \\
&= (F_1 + F_2)^2q^2\left(g^{\mu\nu} - \frac{q^{\mu}q^{\nu}}{q^2}\right) + \left(F_1^2 - \frac{q^2}{4M^2}F_2^2\right)(q + 2p)^{\mu}(q + 2p)^{\nu}.
\end{aligned} \tag{C.26}$$

C.4 Tensor contraction

The leptonic and hadronic tensors can be contracted:

$$\begin{aligned}
L_{\mu\nu}H^{\mu\nu} &= 2(k'_{\mu}k_{\nu} + k'_{\nu}k_{\mu} - g_{\mu\nu}k' \cdot k) \\
&\quad \times \left[(F_1 + F_2)^2q^2\left(g^{\mu\nu} - \frac{q^{\mu}q^{\nu}}{q^2}\right) + \left(F_1^2 - \frac{q^2}{4M^2}F_2^2\right)(q + 2p)^{\mu}(q + 2p)^{\nu} \right]
\end{aligned} \tag{C.27}$$

One can use the fact that the leptonic current is conserved and drop any contractions of the form $q^{\mu}L_{\mu\nu} = q^{\nu}L_{\mu\nu} = 0$. The formula reads

$$\begin{aligned}
L_{\mu\nu}H^{\mu\nu} &= 2(F_1 + F_2)^2q^2(-2k' \cdot k) + 2\left(F_1^2 - \frac{q^2}{4M^2}F_2^2\right)4\left[2(k' \cdot p)(k \cdot p) - M^2k' \cdot k\right] \\
&= 2(F_1 + F_2)^2q^4 + 8\left(F_1^2 - \frac{q^2}{4M^2}F_2^2\right)\left[2(k' \cdot p)(k \cdot p) + \frac{q^2}{2}M^2\right],
\end{aligned} \tag{C.28}$$

where the equality $q^2 = (k' - k)^2 = -2k' \cdot k$ has been used.

Bibliography

- [1] W. Pauli. Dear radioactive ladies and gentlemen. *Phys. Today*, 31N9:27, 1978.
- [2] C. L. Cowan, F. Reines, F. B. Harrison, H. W. Kruse, and A. D. McGuire. Detection of the free neutrino: A Confirmation. *Science*, 124:103–104, 1956.
- [3] S. M. Bilenky. Neutrino. History of a unique particle. *Eur. Phys. J.*, H38:345–404, 2013.
- [4] B. Pontecorvo. Mesonium and anti-mesonium. *Sov. Phys. JETP*, 6:429, 1957. [Zh. Eksp. Teor. Fiz.33,549(1957)].
- [5] B. Pontecorvo. Inverse beta processes and nonconservation of lepton charge. *Sov. Phys. JETP*, 7:172–173, 1958. [Zh. Eksp. Teor. Fiz.34,247(1957)].
- [6] Y. Fukuda et al. Evidence for oscillation of atmospheric neutrinos. *Phys. Rev. Lett.*, 81:1562–1567, 1998.
- [7] Q. R. Ahmad et al. Measurement of the rate of $\nu_e + d \rightarrow p + p + e^-$ interactions produced by 8B solar neutrinos at the Sudbury Neutrino Observatory. *Phys. Rev. Lett.*, 87:071301, 2001.
- [8] Q. R. Ahmad et al. Direct evidence for neutrino flavor transformation from neutral current interactions in the Sudbury Neutrino Observatory. *Phys. Rev. Lett.*, 89: 011301, 2002.
- [9] M. H. Ahn et al. Measurement of Neutrino Oscillation by the K2K Experiment. *Phys. Rev.*, D74:072003, 2006.
- [10] K. Abe et al. Indication of Electron Neutrino Appearance from an Accelerator-produced Off-axis Muon Neutrino Beam. *Phys. Rev. Lett.*, 107:041801, 2011.

-
- [11] A. A. Aguilar-Arevalo et al. A Search for electron neutrino appearance at the $\Delta m^2 \sim 1\text{eV}^2$ scale. *Phys. Rev. Lett.*, 98:231801, 2007.
- [12] P. Adamson et al. Improved search for muon-neutrino to electron-neutrino oscillations in MINOS. *Phys. Rev. Lett.*, 107:181802, 2011.
- [13] M. Antonello et al. Search for anomalies in the ν_e appearance from a ν_μ beam. *Eur. Phys. J.*, C73:2599, 2013.
- [14] M. J. Frank. First Neutrino Oscillation Results from NO ν A. 2016. URL <http://lss.fnal.gov/archive/2016/conf/fermilab-conf-16-127-nd.pdf>.
- [15] C. Adams et al. The Long-Baseline Neutrino Experiment: Exploring Fundamental Symmetries of the Universe. 2013.
- [16] K. Abe et al. Physics potential of a long-baseline neutrino oscillation experiment using a J-PARC neutrino beam and Hyper-Kamiokande. *PTEP*, 2015:053C02, 2015.
- [17] A. A. Aguilar-Arevalo et al. First Measurement of the Muon Neutrino Charged Current Quasielastic Double Differential Cross Section. *Phys. Rev.*, D81:092005, 2010.
- [18] M. Martini, M. Ericson, G. Chanfray, and J. Marteau. A Unified approach for nucleon knock-out, coherent and incoherent pion production in neutrino interactions with nuclei. *Phys. Rev.*, C80:065501, 2009.
- [19] R. Acciarri et al. Detection of back-to-back proton pairs in charged-current neutrino interactions with the ArgoNeuT detector in the NuMI low energy beam line. *Phys. Rev.*, D90(1):012008, 2014.
- [20] Kazuhiro Terao. MicroBooNE: Liquid Argon TPC at Fermilab. *JPS Conf. Proc.*, 8:023014, 2015.
- [21] Kajetan Niewczas and Jan T. Sobczyk. Search for nucleon-nucleon correlations in neutrino-argon scattering. *Phys. Rev.*, C93(3):035502, 2016.
- [22] Kajetan Niewczas. Nucleus probing for short-range correlations using neutrino-nucleon interactions. In *Proceedings, 15th International Conference on Strangeness in Quark Matter (SQM 2015): Dubna, Moscow region, Russia, July 6-11, 2015*, volume 668, page 012119, 2016.

- [23] Tomasz Golan, Cezary Juszczak, and Jan T. Sobczyk. Final State Interactions Effects in Neutrino-Nucleus Interactions. *Phys. Rev.*, C86:015505, 2012.
- [24] J. D. Walecka. *Electron scattering for nuclear and nucleon structure*. Cambridge University Press, 2005. ISBN 9780511034831, 9780521780438, 9780521018395.
- [25] Michael E. Peskin and Daniel V. Schroeder. *An Introduction to quantum field theory*. 1995. ISBN 9780201503975, 0201503972. URL <http://www.slac.stanford.edu/spires/find/books/www?cl=QC174.45%3AP4>.
- [26] K. A. Olive et al. Review of Particle Physics. *Chin. Phys.*, C38:090001, 2014.
- [27] S.D. Drell and F. Zachariasen. *Relativistic quantum mechanics*. Oxford University Press, 1961. URL <https://archive.org/details/electromagnetics002214mbp>.
- [28] F. J. Ernst, R. G. Sachs, and K. C. Wali. Electromagnetic form factors of the nucleon. *Phys. Rev.*, 119:1105–1114, 1960.
- [29] C. F. Perdrisat, V. Punjabi, and M. Vanderhaeghen. Nucleon Electromagnetic Form Factors. *Prog. Part. Nucl. Phys.*, 59:694–764, 2007.
- [30] S. Frullani and J. Mougey. Single Particle Properties of Nuclei Through (e, e' p) Reactions. *Adv. Nucl. Phys.*, 14:1–283, 1984.
- [31] D. H. E. Gross and R. Lipperheide. Quasi-free scattering processes and the hole structure of atomic nuclei. *Nucl. Phys.*, A150:449–460, 1970.
- [32] Artur M. Ankowski and Jan T. Sobczyk. Construction of spectral functions for medium-mass nuclei. *Phys. Rev.*, C77:044311, 2008.
- [33] J. A. Caballero, T. W. Donnelly, E. Moya de Guerra, and J. M. Udias. Analysis of factorization in (e, e-prime p) reactions: A Survey of the relativistic plane wave impulse approximation. *Nucl. Phys.*, A632:323–362, 1998.
- [34] Omar Benhar, Alessandro Lovato, and Noemi Rocco. Contribution of two-particle–two-hole final states to the nuclear response. *Phys. Rev.*, C92(2):024602, 2015.
- [35] E. J. Moniz, I. Sick, R. R. Whitney, J. R. Ficenec, Robert D. Kephart, and W. P. Trower. Nuclear Fermi momenta from quasielastic electron scattering. *Phys. Rev. Lett.*, 26:445–448, 1971.

-
- [36] D. Rohe et al. Correlated strength in nuclear spectral function. *Phys. Rev. Lett.*, 93:182501, 2004.
- [37] J. Arrington, D. W. Higinbotham, G. Rosner, and M. Sargsian. Hard probes of short-range nucleon-nucleon correlations. *Prog. Part. Nucl. Phys.*, 67:898–938, 2012.
- [38] Noemi Rocco, Alessandro Lovato, and Omar Benhar. Unified description of electron-nucleus scattering within the spectral function formalism. *Phys. Rev. Lett.*, 116(19):192501, 2016.
- [39] Omar Benhar and Adelchi Fabrocini. Two nucleon spectral function in infinite nuclear matter. *Phys. Rev.*, C62:034304, 2000.
- [40] Camille Colle, Wim Cosyn, Jan Ryckebusch, and Maarten Vanhalst. Factorization of exclusive electron-induced two-nucleon knockout. *Phys. Rev.*, C89(2):024603, 2014.
- [41] Tom Van Cuyck, Natalie Jachowicz, Raúl González-Jiménez, Marco Martini, Vishvas Pandey, Jan Ryckebusch, and Nils Van Dessel. Influence of short-range correlations in neutrino-nucleus scattering. *Phys. Rev.*, C94(2):024611, 2016.
- [42] C. Anderson et al. The ArgoNeuT Detector in the NuMI Low-Energy beam line at Fermilab. *JINST*, 7:P10019, 2012.
- [43] Jakub Żmuda, Krzysztof M. Graczyk, Cezary Juszczak, and Jan T. Sobczyk. NuWro Monte Carlo generator of neutrino interactions - first electron scattering results. *Acta Phys. Polon.*, B46(11):2329, 2015.
- [44] L. L. Salcedo, E. Oset, M. J. Vicente-Vacas, and C. Garcia-Recio. Computer Simulation of Inclusive Pion Nuclear Reactions. *Nucl. Phys.*, A484:557–592, 1988.
- [45] V. R. Pandharipande and Steven C. Pieper. Nuclear transparency to intermediate-energy nucleons from $(e, e'p)$ reactions. *Phys. Rev.*, C45:791–798, 1992.
- [46] K. M. Graczyk, D. Kielczewska, P. Przewlocki, and J. T. Sobczyk. $C(5)^{**}A$ axial form factor from bubble chamber experiments. *Phys. Rev.*, D80:093001, 2009.
- [47] Jan T. Sobczyk. and Jakub Zmuda. Impact of nuclear effects on weak pion production at energies below 1 GeV. *Phys. Rev.*, C87(6):065503, 2013.

-
- [48] Cezary Juszczak, Jaroslaw A. Nowak, and Jan T. Sobczyk. Simulations from a new neutrino event generator. *Nucl. Phys. Proc. Suppl.*, 159:211–216, 2006. [,211(2005)].
- [49] Jan T. Sobczyk and Jakub Żmuda. Investigation of recent weak single-pion production data. *Phys. Rev.*, C91(4):045501, 2015.
- [50] Jan T. Sobczyk. Multinucleon ejection model for Meson Exchange Current neutrino interactions. *Phys. Rev.*, C86:015504, 2012.
- [51] Tomasz Golan. A comparison of Monte Carlo generators. *AIP Conf. Proc.*, 1663:030003, 2015.
- [52] R. Acciarri et al. A study of electron recombination using highly ionizing particles in the ArgoNeuT Liquid Argon TPC. *JINST*, 8:P08005, 2013.
- [53] E. Bellotti, D. Cavalli, and C. Matteuzzi. Positive-pion absorption by c nuclei at 130 mev. *Nuovo Cim.*, A18:75–93, 1973.
- [54] J.D. Bjorken and S.D. Drell. *Relativistic quantum mechanics*. International series in pure and applied physics. McGraw-Hill, 1964. URL <https://books.google.pl/books?id=pAdRAAAAMAAJ>.